Orbital angular momentum: origins, behavior and applications

Alison M. Yao[1] and Miles J. Padgett[2]

[1]SUPA and Department of Physics, University of Strathclyde, Glasgow G4 0NG, Scotland, UK

[2]Department of Physics and Astronomy, SUPA, Kelvin Building, University of Glasgow, Glasgow G12 8QQ, Scotland, UK (m.padgett@physics.gla.ac.uk)

Received October 8, 2010; revised January 5, 2011; accepted January 5, 2011; published May 15, 2011 (Doc. ID 136333)

As they travel through space, some light beams rotate. Such light beams have angular momentum. There are two particularly important ways in which a light beam can rotate: if every polarization vector rotates, the light has *spin*; if the phase structure rotates, the light has *orbital angular momentum* (OAM), which can be many times greater than the spin. Only in the past 20 years has it been realized that beams carrying OAM, which have an optical vortex along the axis, can be easily made in the laboratory. These light beams are able to spin microscopic objects, give rise to rotational frequency shifts, create new forms of imaging systems, and behave within nonlinear material to give new insights into quantum optics.

OCIS codes: 050.4865, 260.6042

1943-8206/11/020161-44/$15.00

Orbital angular momentum: origins, behavior and applications

Alison M. Yao and Miles J. Padgett

1. The Origins and History of Orbital Angular Momentum

1.1. Electromagnetic Fields to Carry Angular Momentum

Most scientists realize that light carries a linear momentum equivalent to $\hbar k_0$ per photon and, if circularly polarized, a spin angular momentum (SAM) of $\pm\hbar$ per photon. In 1992, Allen *et al.* recognized that light beams with an azimuthal phase dependence of $\exp(i\ell\phi)$ carry an *orbital* angular momentum (OAM) that can be many times greater than the spin [1] and that such beams were readily realizable. This OAM is completely distinct from the familiar SAM, most usually associated with the photon spin, that is manifest as circular polarization [2]; see Fig. 1.

The relationship between linear and angular momentum is a simple one; $\mathbf{L} = \mathbf{r} \times \mathbf{p}$, where $\mathbf{r}$ is the particle's position from the origin, $\mathbf{p} = m\mathbf{v}$ is its linear momentum, and $\times$denotes the cross product. For example, a laser pointer shone at a door can exert a torque about the hinge, albeit not usually enough to open it! However, when we discuss orbital angular momentum we refer instead to an angular momentum component parallel to the propagation direction, z, and hence for which $\mathbf{r} \times \mathbf{p}$ is notionally zero [3]. In relation to the door example given above, we seek to identify an angular momentum capable of twisting the door knob.

Any angular momentum component in the z direction, by definition, requires a component of linear momentum in the x, y plane, i.e., a light beam with transverse momentum components. The angular momentum density, $\mathbf{j}$, is related to the linear momentum density $\mathbf{p} = \varepsilon_0 \mathbf{E} \times \mathbf{B}$ through $\mathbf{j} = \mathbf{r} \times \mathbf{p}$, where ε_0 is the dielectric permittivity, and $\mathbf{E}$ and $\mathbf{B}$ are the electric and magnetic fields, respectively. The linear momentum of a transverse plane wave is then in the propagation direction, z, and there cannot be any component of angular momentum in the same direction. Hence it follows that, at the most fundamental level, an angular momentum in the z direction requires a component of the electric and/or magnetic field also in the z direction. One sees immediately that, even if circularly polarized, a plane wave cannot carry an angular momentum of any type. This last statement has led to some debate, but the resolution of this seeming paradox is simply that the perfect plane wave is only ever found in textbooks. Real beams are limited in extent either by the beams themselves or by the measurement system built to observe

Figure 1

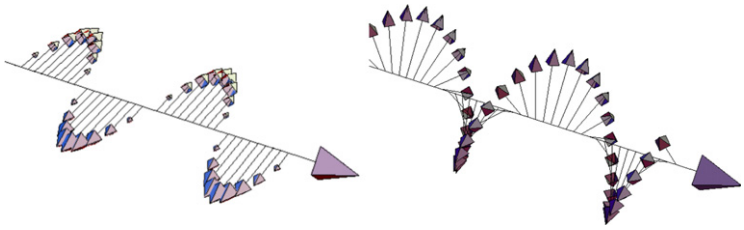

The spin angular momentum (SAM) of light is connected to the polarization of the electric field. Light with linear polarization (left) carries no SAM, whereas right or left circularly polarized light (right) carries a SAM of $\pm\hbar$ per photon.

them, and this finite aperture always gives rise to an axial component of the electromagnetic field [4]. For the case of circular polarization, the axial component of the electromagnetic field is an unavoidable consequence of the radial gradient in intensity that occurs at the edge of the beam or the measurement system. A detailed treatment of these edge effects, for any arbitrary geometry, always returns a value of the angular momentum, when integrated over the whole beam, of $\pm\hbar$ per photon [4] for right-handed and left-handed circular polarization, respectively.

Strangely, the origin of OAM is easier to understand. The simplest example of a light beam carrying OAM is one with a phase in the transverse plane of $\phi(r, \phi) = \exp(i\ell\phi)$, where ϕ is the angular coordinate and ℓ can be any integer value, positive or negative. As shown in Fig. 2, such beams have helical phase fronts with the number of intertwined helices and the handedness depending on the magnitude and the sign of ℓ, respectively ($\ell = 3$ corresponds to a pasta fusilli). One can see immediately that an electromagnetic field transverse to these phase fronts has axial components. Equivalently, the Poynting vector, which is at all times parallel to the surface normal of these phase fronts, has an azimuthal component around the beam and hence an angular momentum along the beam axis.

It was a breakthrough of the 1992 paper [1] that they recognized that all helically phased beams carried an OAM equivalent to a value of $\ell\hbar$ per photon. However, perhaps what is most surprising is not that helically phased beams carry an angular momentum—a simple ray-optical picture suggests just that from the azimuthal component of the momentum flow—but that this OAM, just like spin, should be in units of $\hbar$.

That the OAM should be quantized in units of $\hbar$ follows from a simple geometrical argument. At a radius r, the inclination of the phase front, and hence of the Poynting vector, with respect to the beam axis is simply $\ell\lambda/2\pi r$. This, in turn, sets the azimuthal component of the light's linear momentum as $\hbar k_0 \ell\lambda/2\pi r$ per photon [5], which, when multiplied by the radius vector, gives an angular momentum of $\ell\hbar$ per photon [6]. For comparison, we note that a circular path of circumference λ has a radius of $\lambda/2\pi$. A linear momentum of $\hbar k_0$ directed around this circle gives an angular momentum of $\hbar$, i.e., the SAM of the photon. Within the

Figure 2

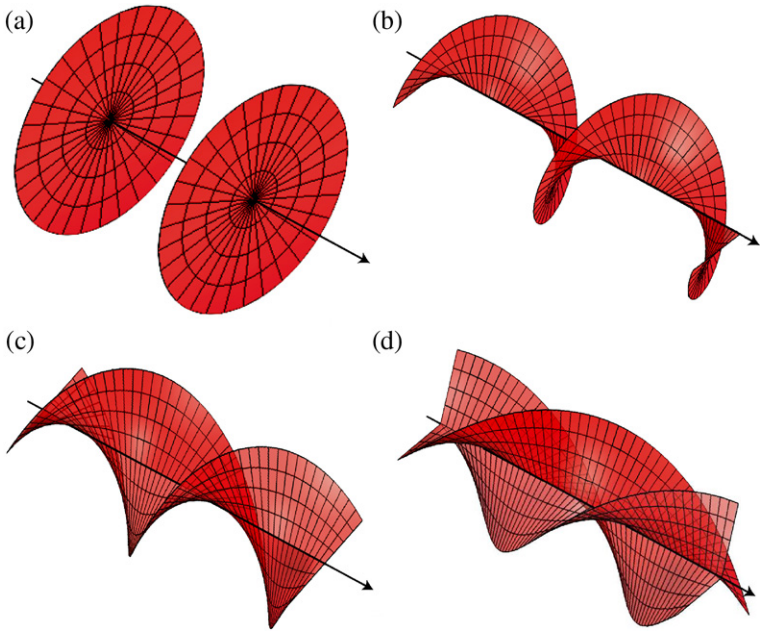

Helical phase fronts for (a) $\ell = 0$, (b) $\ell = 1$, (c) $\ell = 2$, and (d) $\ell = 3$.

paraxial approximation the separation of the angular momenta seems quite straightforward.

Of course, both the orbital and spin angular momenta of light can be derived more formally from Maxwell's equations, which, in the absence of quantization, give an angular momentum to energy ratio of ℓ/ω for a helically phased wave, and σ/ω for a circularly polarized wave, where $\sigma = \pm 1$ for right- and left-handed polarized light, respectively [3]. Assuming that the energy of each photon is $\hbar\omega$, this gives the simple expressions for orbital and spin angular momenta of $\ell\hbar$ and $\sigma\hbar$, as expected. This seemingly clear separation of orbital and spin components is complicated in the presence of tight focusing [7–9], and in such situations one needs to analyze the various components in terms of angular momentum flux [10]. However, in most cases the orbital and spin angular momenta remain distinct quantities and useful concepts with which to analyze many experimental situations.

1.2. History of Spin and Orbital Angular Momenta

Although the detailed study of orbital angular momentum was initiated by Allen *et al.*'s [1] discovery that OAM beams could be easily generated, both SAM and OAM have a history prior to this. Indeed, the SAM of light has a history dating back at least to Poynting in 1909 [11], who anticipated that circularly polarized light should have an angular momentum to energy ratio of $\sigma\hbar$. He proposed that any transformation of the polarization state, say, from linear to circular, must be accompanied by an angular momentum exchange with the optical system. In 1936 Beth [12] was successful in demonstrating this transfer

between polarized light and the rotational motion of a birefringent wave plate suspended on a filament.

The OAM of light also has a history prior to 1992. Most atomic transitions are dipolar, meaning also that the emitted photon can carry $\hbar$ angular momentum. It has been recognized since at least the 1950s that higher-order transitions, e.g., quadrupole, require the emitted light to carry multiple units of $\hbar$ angular momentum, and hence an OAM in addition to the spin [13]. However, it seems that this OAM was always considered to be a displaced linear momentum acting about a radius vector, giving an angular momentum of the type we illustrated with the example of a laser pointer opening a door.

The key point of Allen *et al.* in 1992 [1] was that this OAM was a natural property of all helically phased beams, and hence could be readily generated in a standard optics lab. What makes their discovery even more remarkable is that helically phased light fields had themselves been under study for a number of years without any recognition or reference to their angular momentum. Prior to 1992, perhaps the main source of interest was that the helical phase fronts require a phase singularity running along the center of the beam and hence, at least from a classical perspective, a line of total darkness. However, since the line of singularity carries no energy, it has no momentum either, and hence no angular momentum. Therefore, one emphasizes that the angular momentum arises from the light surrounding the singularity, not the singularity itself.

1.3. Orbital Angular Momentum and Phase Singularities

Within fields, lines of phase singularity had been recognized in the 1930s by Dirac, in his work on the discussion for the requirements to obtain a magnetic monopole [14]. However, with respect to singularities in electromagnetic field, it was Nye and Berry who, in the 1970s, were considering the form of radio echoes reflected from the underside of the Antarctic ice sheet [15]. To simulate this they used ultrasound scattered from a rough surface and noted that the spatial form of the returned signal contained intensity nulls around which the phase of the signal changed by 2π. Undoubtedly it was this identification of phase singularities within randomly scattered fields that inspired the present day interest in phase singularities and optical vortices. Indeed, in 1979 Berry, Nye, and Wright reported the study of phase singularity lines within elegant examples of multiple beam interference [16]. In all of these examples the optical field contained many lines of singularity, of both handedness, mapping out complex three-dimensional topologies. Although the light surrounding each of these lines could be considered to be carrying an angular momentum, the angular momentum over any arbitrary cross section was approximately zero. Possibly the first generation of a beam containing a single line of phase singularity was reported in 1979 by Vaughan and Willets, who examined the interferograms produced when the output from a high-power, krypton-ion laser was interfered with its own mirror image [17]. They deduced that the high-order Hermite–Gaussian modes

Figure 3

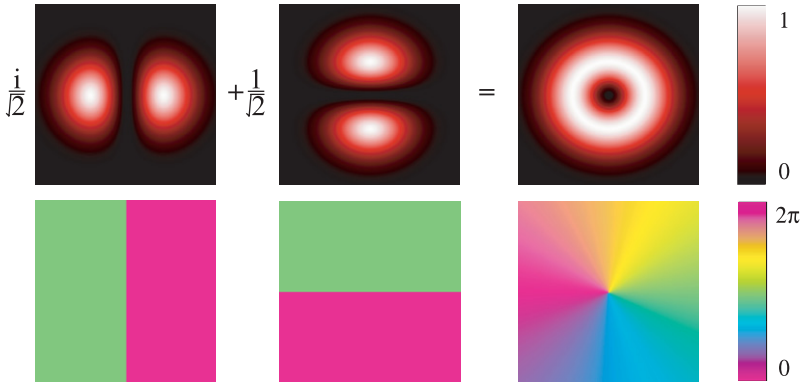

Combination of Hermite–Gaussian modes HG_{01} and HG_{10} to produce a helically phased Laguerre–Gaussian mode (LG_{01}). Top, normalized intensity plots; bottom, corresponding phase profiles.

HG_{01} and HG_{10} could combine to give a helically phased beam, as shown in Fig. 3.

In this early work, what they did not seem to discuss was whether the two modes were frequency degenerate and hence whether the handedness of the helical phase fronts was maintained over time or not. In 1988, Tamm considered a HeNe laser where the careful positioning of an intracavity absorber could encourage the two modes to frequency lock such that they combined to give a helically phased output of one particular handedness [18]. The system was further refined, in 1990, such that the sense of the helical phase was bistable [19]. Simultaneously, spontaneous breaking of the cylindrical symmetry in the output of a laser beam induced by helical modes was described by Lugiato *et al.* in 1989 [20]. This work lead to the identification of "spatial complexity" in multi-transverse-mode lasers [21] where helical modes play a crucial role in the formation of phase singularities [22] and in their dynamics [23,24]. The relevance and importance of Laguerre–Gauss modes in laser dynamics was finally formalized by D'Alessandro and Oppo [25]. In parallel with this work on laser modes, Coullet recognized the mathematical similarity between the description of helically phased beams and superfluid vortices, thereby coining the term "optical vortex" [26].

As an alternative to obtaining these helically phased beams directly as the output from a multimode laser, Soskin and co-workers, in 1990, reported that a simple diffractive optical element, comprising a diffraction grating with fork dislocation centered on the beam axis, could convert the fundamental Gaussian mode from any laser into a helically phased mode [27]. This approach, based on diffractive optics, is now largely the method of choice for producing helically phased beams.

However, optical vortices (phase singularities) are not solely a property of specially prepared laser beams. As discussed, they were identified for the acoustic case in the random scatter from a rough surface [15,28], and optical waves are no different. The interference between three or more randomly directed plane wave components of similar intensity always

Figure 4

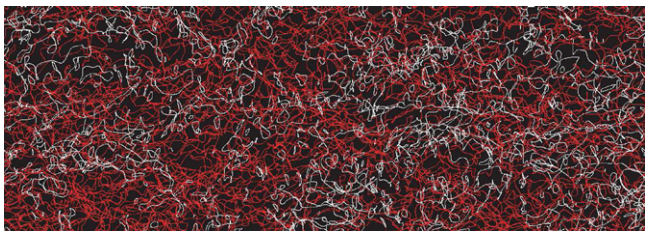

Complex paths of vortex lines form complicated topological features. These can be unbounded (red) or loops (white).

results in a field cross-section containing many vortices [29,30]. The best known example of this is laser speckle, observed whenever an expanded laser beam is scattered from a rough surface; each of the observed dark specks is, in fact, a phase singularity [31]. In three dimensions these vortex lines map out complex paths that are fractal in nature [32] and even form complicated topological features like loops and knots as shown in Fig. 4 [33,34].

Despite all of these examples, however, prior to Allen *et al.* in 1992 [1], none of this early work on naturally occurring or engineered optical vortices recognized that such features could give rise to an angular momentum within a light beam that was additional to, and independent of, that associated with circular polarization and the photon spin. Recent reviews on the subject of OAM include reference to their quantum and classical applications [35,36].

2. Generation of Helically Phased Beams

2.1. Spiral Phase Plates

Perhaps the most obvious approach to the generation of a helically phased beam is to pass a plane wave beam through an optical element with a helical surface, as shown in Fig. 5. The optical thickness of the component increases with azimuthal position according to $\ell\lambda\theta/2\pi(n-1)$, where n is the refractive index of the medium. Although this is a seemingly simple idea, at optical wavelengths this approach requires extreme precision in the pitch of helical surface. In the initial demonstration, a spiral phase plate with a much larger physical step was immersed in an index-matched fluid bath, the temperature of which could be controlled to give precisely the index mismatch required to tune the step height to the operating wavelength [37]. Although spiral phase plates have now been manufactured to directly match the wavelengths for millimeter wave [38] and even optical wavelengths [39,40], they are not the only approach.

The spiral phase plate illustrates nicely why the resulting helically phased beam should carry an OAM and how this is transferred from the optical component to the light [38]. Consider the case of an incident light ray striking the planar face of the phase plate at normal incidence. We

Figure 5

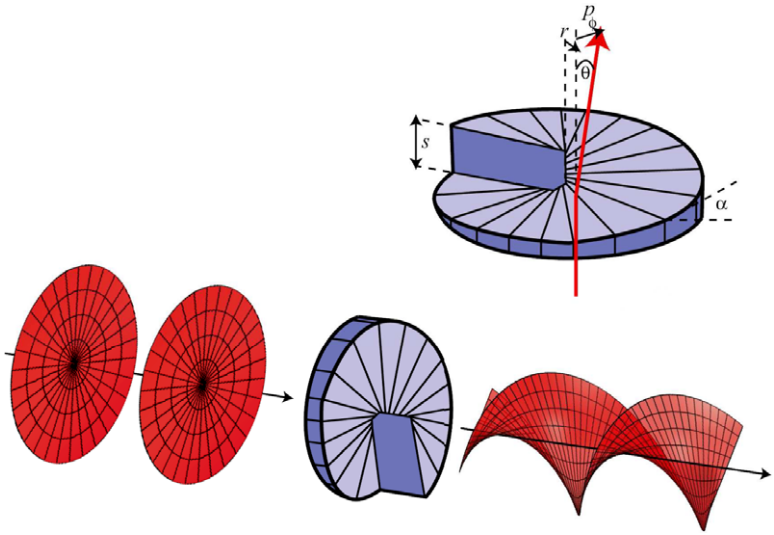

A spiral phase plate can generate a helically phased beam from a Gaussian. In this case $\ell = 0 \rightarrow \ell = 2$.

see that upon exiting the helical face the ray is refracted in the azimuthal direction. Thus the linear momentum of the light acquires an azimuthal component that, when expressed with respect to a radius vector, gives an angular momentum along the beam axis. At a radius r, the azimuthal angle of the helical face is simply $\ell\lambda/2\pi r(n-1)$. The application of Snell's law then gives the angular deviation in the transmitted ray as $(n-1)\ell\lambda/2\pi r(n-1) = \ell/k_0 r$. Multiplying this by the linear momentum per photon, $\hbar k_0$, and the radius vector gives an angular momentum per photon of $\ell\hbar$.

2.2. Laguerre–Gaussian Modes

Helically phased light carries an OAM irrespective of the radial distribution of the beam. However, it is useful to express most beams in a complete basis set of orthogonal modes. For OAM carrying beams this is most usually the Laguerre–Gaussian (LG) mode set; these modes have amplitude distributions, $LG_{p\ell}$, given by [3,41,42]

$$LG_{p\ell} = \sqrt{\frac{2p!}{\pi\,(p+|\ell|)!}}\frac{1}{w(z)}\left[\frac{r\sqrt{2}}{w(z)}\right]^{|\ell|}\exp\left[\frac{-r^2}{w^2(z)}\right]L_p^{|\ell|}\left(\frac{2r^2}{w^2(z)}\right)\exp[i\ell\phi]$$
$$\exp\left[\frac{ik_0r^2z}{2(z^2+z_R^2)}\right]\exp\left[-i(2p+|\ell|+1)\tan^{-1}\left(\frac{z}{z_R}\right)\right] \quad (1)$$

where the $1/e$ radius of the Gaussian term is given by $w(z) = w(0)[(z^2 + z_R^2)/z_R^2]^{1/2}$ with $w(0)$ being the beam waist, z_R the Rayleigh range, and $(2p+|\ell|+1)\tan^{-1}(z/z_R)$ the Gouy phase. $L_p^{|\ell|}(x)$ is an associated Laguerre

Figure 6

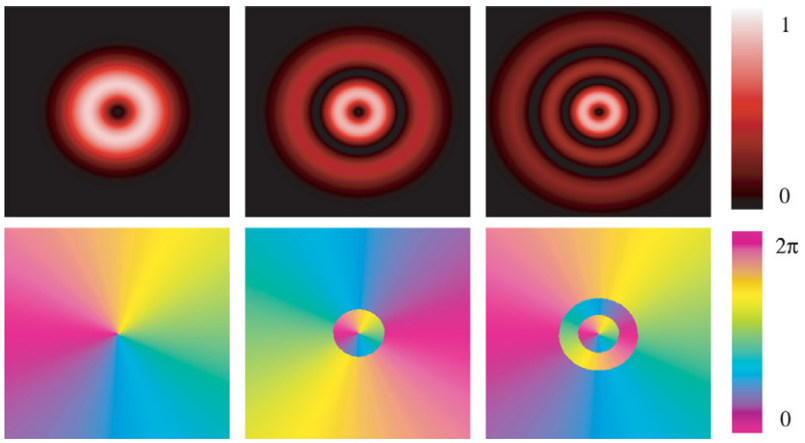

Normalized intensity (top) and phase (bottom) plots of Laguerre–Gaussian modes: LG_{01}, LG_{11}, and LG_{21} (left to right) showing the $p + 1$ concentric rings and the effect on the phase pattern.

polynomial, obtained from the more familiar Laguerre polynomials by

$$L_p^{|\ell|}(x) = (-1)^{|\ell|} \frac{d^{|\ell|}}{dx^{|\ell|}} L_{p+|\ell|}(x), \tag{2}$$

ℓ is the azimuthal index giving an OAM of $\ell\hbar$ per photon, and p is the number of radial nodes in the intensity distribution. In terms of their intensity cross section, an LG mode with $\ell > 0$ comprises $p+1$ concentric rings with a zero on-axis intensity. Figure 6 shows the intensity and phase plots of LG modes LG_{01}, LG_{11}, and LG_{21}. Other beam types that can contain similar phase structure are high-order Bessel [43] and Mathieu [44] beams.

When Laguerre–Gaussian beams interfere they produce vortex structures resulting in complex patterns of bright and dark regions, as shown in Fig. 7.

2.3. Diffractive Optical Elements for Generating Orbital Angular Momentum

As an alternative to making complex refractive optics, diffractive optical elements are readily designed to mimic any refractive element of choice, albeit only at a single wavelength. A helical phase profile $\exp(i\ell\phi)$ converts a Gaussian laser beam into a helical mode whose wave fronts resemble an ℓ-fold corkscrew, as shown in Fig. 8. In practice, the phase distribution of the desired optical component is typically added to a linear phase ramp and the sum expressed as modulo 2π, as shown in Fig. 9. The result is a diffraction grating that produces the desired beam in the first diffraction order. The components are effectively holograms of the desired optical element and are thus often referred to as "computer generated holograms." To produce helical beams these holograms can be either the "forked diffraction gratings" discussed in

Figure 7

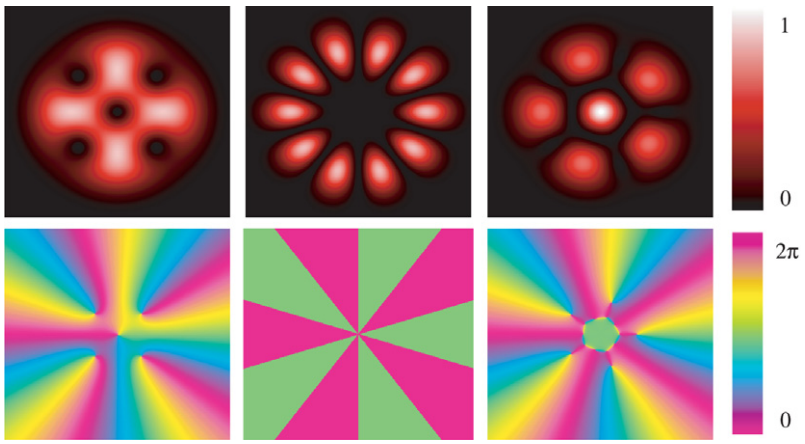

Normalized intensity (top) and phase (bottom) profiles of some superpositions of Laguerre–Gaussian modes: $LG_{01} + LG_{05}$, $LG_{0-5} + LG_{05}$, and $LG_{10} + LG_{05}$ (left to right).

Figure 8

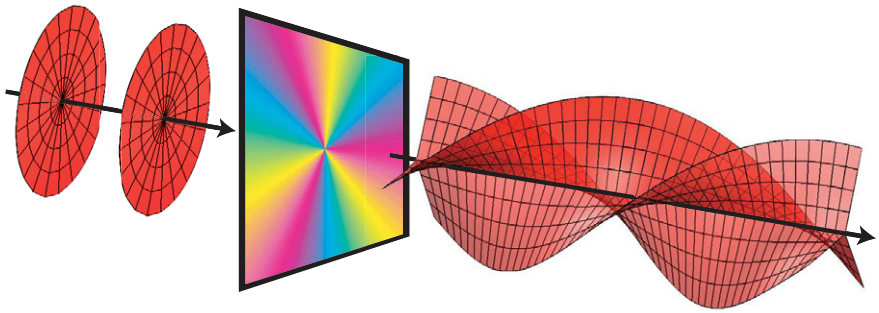

A helical phase profile $\exp(i\ell\phi)$ converts a Gaussian laser beam into a helical mode whose wave fronts resemble an ℓ-fold corkscrew. In this case $\ell = 3$.

Section 1 [27,45,46] or spiral Fresnel lenses [47]. The technique can be easily extended to cover both the ℓ and the p of the generated beams [48]. What makes the holographic approach particularly appealing is the commercial availability of spatial light modulators (SLMs). These are pixellated liquid crystal devices that can be programmed through the video interface of a computer to act as holograms. Changing their design is as simple as changing the image displayed by the computer interfacing the device.

Computer generation of holograms and their implementation for the generation of exotic beams is obviously not restricted to pure helical modes; it is a general technique that can be applied to all complex beam types or their superpositions. However, in general, the hologram design is more complicated than simply that of a phase mask alone. Accurate holograms are the complex far-field diffraction patterns of the desired objects or beams and as such are defined in terms of both their phase and intensity. For many simple beams it is sufficient to define only the

Figure 9

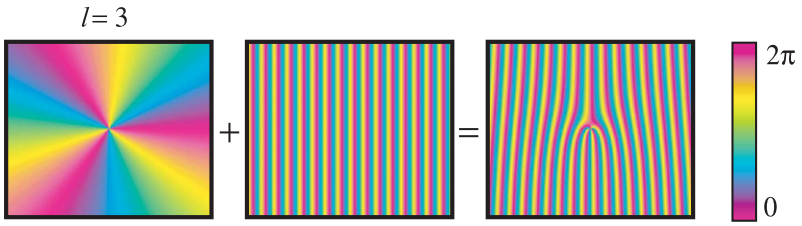

A combination of the phase distribution of the desired optical component (left) plus a linear phase ramp (middle) creates a forked diffraction grating (right), which can produce a helically phased beam. In this case $\ell = 3$.

phase, assuming a uniform illumination, and in such cases the far field (Fourier transform) of the hologram is a close approximation to the target beam. For example, when a forked diffraction grating is illuminated with a fundamental Gaussian beam from a conventional laser of radius w_0 the transmitted beam is a superposition of *LG* modes all with the same ℓ index. These predominantly have $p = 0$, but there is also a small contribution of *LG* modes with higher p [49].

However, if precise control over the p of the resulting mode is needed, then it is necessary for the hologram to define both the phase *and* the intensity of the diffracted light. Unfortunately, SLMs are designed to modify only one or the other. Various approaches are possible, including the use of two SLMs in series: the first uses an algorithm such as Gerchberg–Saxton [50] to create the desired intensity distribution, and the second then adjusts the phase to that of the target beam [51]. This approach is particularly suited to cases where the intensity distribution is extremely localized in the hologram plane. For cases when the situation is less localized, typical of the superpositions between simple modes, a single SLM technique is possible. For diffracting holograms the efficiency with which light is diffracted to the first order depends on the depth of the blazing function, which for maximum efficiency is 2π. Varying this depth over the cross section of the hologram allows the intensity at various positions to be reduced, with any unwanted light being directed into the zero order. This gives the precise control over both phase and intensity that is required, albeit at a reduction in the overall efficiency. This technique was used prior to any interest in OAM [52] but has since been used effectively to create many precise superpositions, including those associated with the generation of vortex lines, which are themselves linked and knotted [53,54], or precise modal measurements in quantum entanglement [55].

2.4. Mode Converters Formed from Cylindrical Lenses

Despite the present day ubiquitous use of holograms to produce OAM beams, they were not the method used by Allen *et al.* in 1992 [1]. They, instead, recognized that a specific design of cylindrical lens telescope would transform between Hermite–Gaussian (*HG*) and *LG* modes. The production of *LG* modes using mode converters is based on the fact that an *HG* mode at 45° can be decomposed into a set of *HG* modes

Figure 10

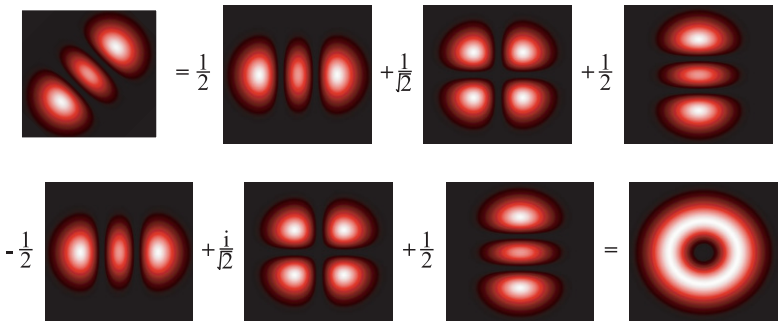

Combining Hermite–Gaussian modes to produce Laguerre–Gaussian modes. An *HG* mode at 45° can be decomposed into a set of *HG* modes, and this same set of *HG* modes, when rephased, can combine to form a particular *LG* mode: $\frac{-1}{2}HG_{02} + \frac{i}{\sqrt{2}}HG_{11} + \frac{1}{2}HG_{20} = LG_{02}$.

and that this same set of *HG* modes, when rephased, can combine to form a particular *LG* mode. The rephasing occurs because as each *HG* mode is focused by the lenses it undergoes a different Gouy phase shift depending on its mode indices and orientation with respect to the cylindrical lenses. A general prescription for transforming combinations of *HG* modes into any particular *LG* mode is given in [56], and an example is shown in Fig. 10, where three *HG* modes are combined to give the Laguerre–Gaussian mode LG_{02}.

The cylindrical lens mode converters have two main forms: the $\pi/2$-converter and the π-converter, as shown in Fig. 11. The $\pi/2$-converter transforms any incident *HG* mode of indices m, n, oriented at 45° to the cylindrical axis of the lens, into an *LG* mode with indices $\ell = m - n$ and $p = \min(m, n)$. The π-converter, on the other hand, transforms any mode into its own mirror image and is optically equivalent to a Dove prism [57]. These cylindrical lens converters are mathematically analogous to the action on polarization of a birefringent $\lambda/4$ plate and a $\lambda/2$ plate, respectively. Their advantage over holograms is that the optical efficiency of conversion is much higher, limited only by the quality of the antireflection coatings of the lenses.

2.5. Coherence Requirements for Beams Carrying Orbital Angular Momentum

One is familiar with the fact that a pure polarization state can be both spatially and temporally incoherent; e.g., it is possible to polarize the light emitted from a tungsten bulb. We should expect OAM to be different, since the very description of a helical phase front implies a coherence of phase across the beam. However, it is still possible to illuminate either a spiral phase plate or a forked diffraction grating with an incoherent source. We first consider a spatially incoherent source as an extended disc illuminating a spiral phase plate, as in Fig. 12. Swartzlander and Hernandez-Aranda [58] showed that the properties of

Figure 11

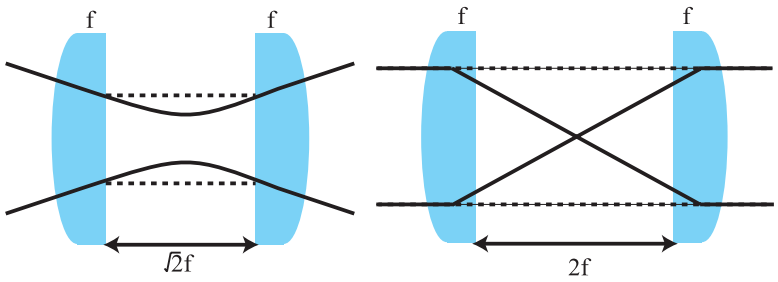

$\pi/2$ and π-converters.

Figure 12

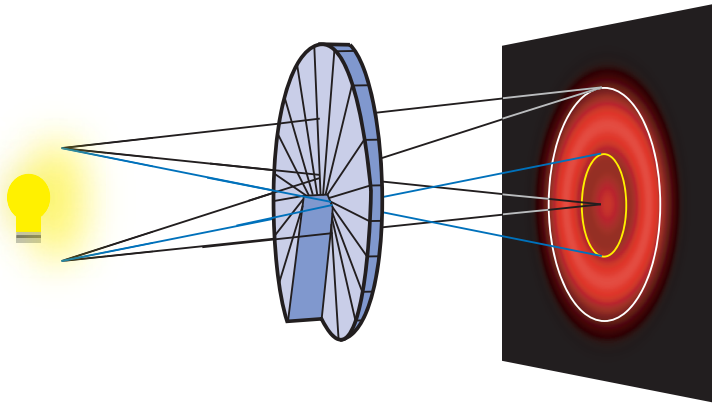

An extended incoherent light source illuminating a spiral phase plate produces a vortex beam with a nonzero on-axis intensity.

the resulting beam can be divided into various annular regions. At small radii one can project a series of rays though the center of the spiral phase plate. This creates a region of vortices in the far field that are incoherent with respect to one other, such that the time-averaged intensity is not zero. The azimuthal energy and momentum flow per photon has an average value that is proportional to the radius, as with a solid body. At larger radii the helical phase fronts produced by each source element are similar and the azimuthal energy and momentum flow per photon is similar to a normal vortex beam, with a value inversely proportional to the radius. Whether a light source gives a vortex beam with a zero or nonzero on-axis intensity is thus an indication of its spatial coherence. Such incoherent vortices have similarities with fluid vortices, which have central regions of lower angular momentum and have been referred to as Rankine vortices [58]. Placing a detector on, or near, the beam axis allows the examination of the light from an extended source while filtering out an intense background from a point source. This forms the basis of an innovative coronograph [59,60] also developed by Swartzlander to potentially spot the light from dim planets in orbit near a much brighter star.

Figure 13

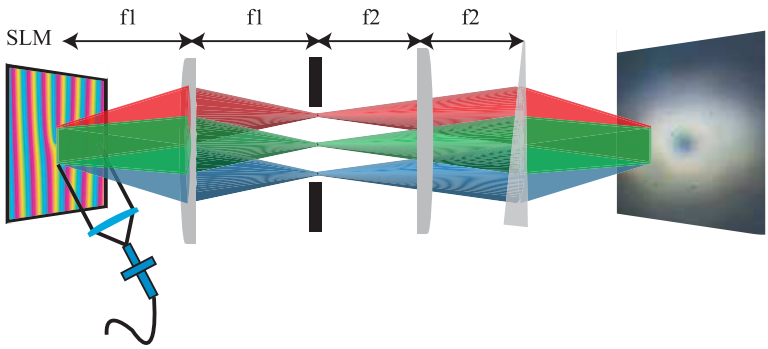

Illumination of a forked diffraction grating with a source with a broad spectral bandwidth results in a white-light vortex.

Even if the light source is spatially coherent it may still have a broad spectral bandwidth, as in white light. Scattered white light does not give a noticeable speckle pattern; however, each spectral component within the bandwidth does. These speckles tend to go unnoticed, since the condition for destructive interference is met by the different components at different positions and it is extremely unlikely that the speckles from all the spectral components will overlap. White-light diffraction from simple apertures results in a spectrally rich pattern [61], where specific wavelengths destructively interfere to give an overall distribution perceived as light's complimentary colors [62]. The step height of a spiral phase plate is designed for only one spectral component and therefore works correctly only with monochromatic light. Similarly, a forked diffraction grating introduces an angular dispersion between the various spectral components. For optical vortices, the separation of the vortices for each spectral component may only be slight, giving a characteristic transition from cyan, to magenta, to yellow [63]. These patterns can be observed in the diffraction of light from a forked diffraction grating or, alternatively, the angular deviation of the different wavelengths can be compensated by the introduction of a prism [64]. The result is a white-light beam with each spectral component having helical phase fronts about a common beam axis, as in Fig. 13. For polychromatic light, the hologram is perhaps the most interesting, as a second dispersive component can be introduced to compensate for the angular dispersion while maintaining the helical phase dependence for every spectral component.

2.6. Orbital Angular Momentum beyond Light

The vast majority of the research in optical vortices and OAM has been carried out in the optical region of the spectrum; however, the phenomenon is obviously not restricted to that. The early work on the rotational Doppler shift [65] (see below) was performed at millimeter-wave frequencies where the longer wavelength relaxed the mechanical precision needs for the alignment. The OAM was introduced to the millimeter-wave beam by using a spiral phase plate made from

Teflon with a step height of 10 mm [38]. Even longer wavelengths, radio waves, are being considered for possible applications in astronomy or RF communications where the helical phase fronts can be detected by using an antenna array [66]. At these longer wavelengths it is possible to create coherent arrays of emitters, each of which can be phase controlled to create a beam with any complex phase front, e.g., helical. In many ways, these phased arrays for detection and generation can be considered to perform a function similar to that of the SLMs used at optical frequencies.

At the other end of the spectrum, diffractive optics have been positioned in the output beam from a synchrotron light source to create an x-ray vortex in its output. It may be that such beams find use in providing extra information within x-ray diffraction for the determination of molecular structure [67].

Moving beyond the electromagnetic spectrum, primitive spiral phase plates have been positioned within the beam of an electron microscope, and this may provide some form of edge detection for low-contrast imaging [68]. Most recently, the creation of vortex electron beams making use of a versatile holographic reconstruction technique in a transmission electron microscope has been shown [69]. This technique demonstrates a reproducible method of creating vortex electron beams in a conventional electron microscope and their use in electron energy-loss spectroscopy to detect the magnetic state of materials and describe their properties. The phased array of transmitters has another obvious embodiment, namely, acoustic loud speakers. A ring of loud speakers each driven at the same frequency but with a phase of $\exp(i\ell\phi)$ produces a helically phased beam, carrying OAM [70,71], in a longitudinal wave system that has no transverse polarization and therefore no possibility of carrying SAM.

3. Interaction of Helically Phased Beams with Matter

3.1. Observing the Angular Momentum of Light

Just as Beth was able to observe the SAM predicted by Poynting, an important step was to observe the transfer of OAM to matter. Initial efforts were directed at observing the reaction torque on the cylindrical lens mode converter itself. Sadly, however, to date this has proved to be too technically demanding. An alternative approach was demonstrated in 1995 based on optical tweezers. Traditionally, optical tweezers use tightly focused beams of light to trap microscopic particles in three dimensions within a surrounding fluid. One notes that for a particle of radius r its mass scales as r^3 while its rotational moment of inertia scales as r^5. Consequently, when the size of the test particle is reduced, it becomes easier to move, but even easier to rotate. Figure 14 shows how a particle is trapped in a circularly polarized beam (left) or in a high-order Laguerre–Gaussian beam (right). In the original experiment micrometer-sized graphite particles were illuminated by a tightly focused LG beam with $\ell = 3$ [72]. Absorption of light, and its angular momentum, caused the particle to rotate at several hertz, and this was correctly attributed to the transfer of OAM from light to matter. Such a transfer of angular momentum and the corresponding

Figure 14

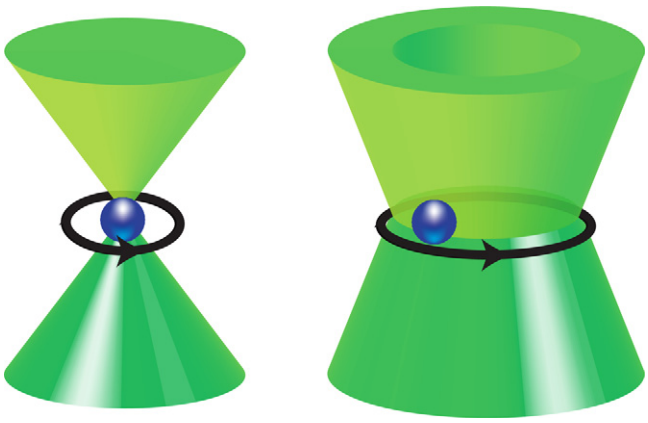

Transfer of angular momentum in optical tweezers. A trapped object can be rotated either by the transfer of SAM from a circularly polarized beam (left) or by the transfer of OAM from a high-order Laguerre–Gaussian beam.

torque on the particle essentially converts the optical tweezers into an optical spanner or wrench. Later experiments used helically phased beams that were also circularly polarized such that they contained both OAM and SAM components. The helical beam was $\ell = 1$ so that its total angular momentum (spin + orbital) could be set at $\hbar + \hbar = 2\hbar$ or $\hbar - \hbar = 0$ depending on the relative handedness of the spin and orbital terms. Initially using a beam in which the spin and orbital term were additive, the partial absorption of the light by a micrometer-sized Teflon particle set it into rotation. Inserting a $\lambda/2$ plate to reverse the sense of the SAM gave a beam with zero total angular momentum and, although the particle remained trapped, it ceased to rotate [73]. The ability to stop the particle in this way reinforced the idea that a Laguerre–Gaussian mode with an azimuthal mode index $\ell = 1$ has a well-defined OAM corresponding to $\hbar$ per photon and that both the spin and OAM have been transferred to the medium. The manipulation of microscopic objects using optical tweezers has now been transformed by the commercial availability of SLM's that have photographically produced optics and allow the generation of multiple traps at arbitrary positions with complex spot spread functions [74].

3.2. Mechanisms for Angular Momentum Transfer

It is generally believed that OAM and SAM are independent when light propagates in or through a homogeneous and isotropic transparent medium, and therefore do not interconvert. However, it has been demonstrated that SAM-to-OAM transfer can indeed occur in such media when a Gaussian beam [9] or circularly polarized vortex beam [8] is tightly focused through a high-numerical-aperture (NA) lens. The observed equivalence of OAM and SAM in these "optical spanners" [75] is also somewhat misleading. The equivalence of OAM and SAM breaks down in a number of ways.

The mechanisms for transfer of OAM and SAM are not the same. In these early demonstrations the transfer mechanism for OAM arose from the absorption of the light for which, at the macroscopic scale, the orbital and spin components are indeed indistinguishable. However, whereas birefringence converts circular to linear polarization and hence changes the SAM causing a birefringent particle to spin [76], it does not change the helical phase fronts and hence does not interact with the OAM. By contrast, astigmatism does change the helical phase fronts and couples to the OAM of the beam, but has no effect upon the polarization and SAM.

The spatial distribution of the orbital and the spin angular momentum is also different. Even the effects of absorption of the OAM and the SAM can differ when the optical beam is large compared with the size of the particle. For example, on an atomic level the SAM can excite a sigma Zeeman transition, whereas the OAM cannot. Even at a larger scale one observes two distinct forms of angular momentum transfer, for example, when a small particle is introduced off-axis to a larger, circularly polarized, helically phased beam. Each point in the beam is circularly polarized, and hence a small birefringent particle experiences a torque, causing it to spin around its own axis. However, when sampled over a small, off-axis, region, the helical phase fronts appear as a plane wave inclined with respect to the optical axis. A small particle experiences a scattering force that has an azimuthal component, leading, in many cases, to an orbiting of the particle around the axis of the beam [77]. A further variant on the use of *LG* beams for rotational control comes from interfering such a beam with its own mirror image to produce an annular interference pattern. Shifting the relative phase of the beam causes the pattern to rotate, thereby rotating the object(s) trapped within [78].

By considering the energy $\hbar\omega$, momentum $\hbar k_0$, and angular momentum $(\sigma + \ell)\hbar$ of the photon one sees that the linear momentum is inversely proportional to the phase velocity and that the angular momentum is inversely proportional to the frequency. Neither of these scalings are uniquely photon properties, and both apply to waves of all types, i.e., not just electromagnetic. Moving beyond light, sound has a frequency $\approx 10^{12}$ times smaller than light and consequently can exert a torque sufficient to rotate macroscopic bodies tens of millimeters in diameter [71]. Even in optical systems, the relationship to the phase velocity means that upon entering a medium with a negative index of refraction one expects the angular momentum to reverse in sign [79]—an effect that might be interesting to observe.

3.3. Optical Momentum to Drive Micromachines

Irrespective of whether it be SAM or OAM, or of the precise transfer mechanism, the maximum torque that can be exerted by any optical beam on a small particle of radius r is of order $\hbar k_0 r$ [80]. Nevertheless, on the scale of a few micrometers and powers of hundreds of milliwatts, rotation speeds can reach hundreds of hertz. Such motion is very suggestive of a micromachine or pump. Early work on micromachines predates the work using angular momentum. Miniature "windmills"

were micromachined from silicon dioxide and held in optical tweezers. The scattering of the light from the rotors exerted a reaction torque, causing their rotation [81]. At a very basic level one can consider this the introduction to the scattered light of an (ill-defined) OAM, but simple azimuthal scattering is perhaps a less complicated explanation. The appealing feature of an all optical approach is that the trapping force creates an "axle" for the device that can never wear out!

Following the demonstrations of both SAM and OAM transfer, OAM was also used as the driving torque for a micromachine, the advantage over shaped rotors being that the direction of rotation could be controlled by changing the sign of the angular momentum [82]. As an alternative to micromachining the components by using lithographic techniques it is also possible to use photopolymerization, which allows the same optical system to be used both for fabrication of the components and their drive [83].

Perhaps the most obvious micromachine to build is a micropump. An array of beams, each carrying OAM, is used to create a circulation of microparticles that, because of the Stokes drag, induces a fluid flow through the array along which other particles are carried [84]. Alternatively, the SAM can be transferred to two microscopic birefringent particles, causing them to spin in opposite directions on either side of a microfluidic channel, thus creating a flow along the channel [85]. However, the scale of these devices is such that their induced flow rate only amounts to a few tens of cubic micrometers per second, many orders of magnitude less than frequently used even in the smallest of microfluidic systems.

3.4. Orbital Angular Momentum and the Interaction with Cold Atoms

As discussed in Subsection 3.2, whereas circular polarization and its associated SAM play a role in atomic selection rules, OAM does not. Even when compared with a tightly focused beam, the effective cross section of the atom is extremely small; so the helical phase front is locally indistinguishable from an inclined plane wave. An atom interacting with a plane wave propagating in the z direction is subjected to a light pressure force proportional to the wave vector k_z. Thus the absorption by a gas of photons from a particular direction followed by an isotropic spontaneous emission generally results in a recoil of the atoms or molecules away from the incident light. If, however, the beam is helically phased it will have a wave vector k_ϕ and an associated force that, at any distance from the beam axis, will exert a torque on the center of mass of the atom, resulting in a spiral-type recoil [86]. If two counterpropagating beams are used, the axial recoil time averages to zero, while the azimuthal recoil is maintained. Various beam configurations have been considered, and the resulting motion of the atoms or molecules calculated. For example, since the atoms or molecules follow trajectories around the beam axis, this was recognized as leading to a manifestation of the rotational Doppler shift [87].

Leaving aside the phase structure of these beams, the annular intensity profile creates an enclosed dark region, ideal for blue-detuned atom

trapping where the atoms experience a force attracting them to the dark regions at the center of an *LG* or similar beam [88]. Furthermore, the residual light scattering potentially pushes the atoms along the beam, turning the annular beam into an "atom hosepipe" [89]. At a macroscopic level, this is similar to the annular intensity distribution of an *LG* beam being used to trap bubbles in optical tweezers, their low refractive index meaning that the direction of the gradient force is reversed so that they are held at the dark core of the beam, surrounded by light [90].

Finally, although individual atoms or molecules are too small to interact with a sufficient area of a typical helically phased beam to sample the OAM, a Bose–Einstein condensate is not. For example, OAM has been transferred from counterpropagating beams to sodium atoms in a Bose–Einstein condensate by using a two-photon stimulated Raman process [91], and the topological properties of an induced vortex motion can lead to longer storage times [92]. Recently, a new variety of dissipationless fluid behavior was found in microcavities under the optical parametric regime [93]. Metastable persistent polariton superflows sustaining a quantized angular momentum have been observed [93] along with the transfer of angular momentum to the steady-state condensate.

4. Analogous Representation and Effects for Helically Phased and Polarized Beams

4.1. Poincaré Sphere for Orbital Angular Momentum Modes

The perfect transformation of *HG* into *LG* modes that is possible with mode converters based on cylindrical lenses stems from the fact that both *HG* modes and *LG* modes are complete sets; thus any one mode can be synthesized from the correct superposition of modes from the other set. The analogy between OAM and SAM states is most readily understood in the case of $LG_{0,1}$ and $LG_{0,-1}$ states. Adding these two modes together produces an $HG_{1,0}$ mode with an orientation that depends upon the relative phase of the *LG* modes used to create it. This is completely analogous to the addition of right- and left-circularly polarized states that add together to form a linear state. In the case of polarization we are familiar with its representation on the surface of the Poincaré sphere, but, of course, the same geometrical approach can be applied to construct a Bloch sphere for the representation of states within any two-dimensional subspace, and OAM is no exception [94,95]. In both cases a particular polarization or OAM state is represented by a vector from the center to the surface of the sphere. In general terms, a state $|\mathbf{a}\rangle$ can be written as

$$|\mathbf{a}\rangle = \cos\left(\frac{\theta_a}{2}\right)|\ell\rangle + e^{i\phi_a}\sin\left(\frac{\theta_a}{2}\right)|-\ell\rangle, \tag{3}$$

where $\mathbf{a} = (\sin(\theta_a)\cos(\phi_a), \sin(\theta_a)\sin(\phi_a), \cos(\theta_a))$ is a vector with latitude $0 \le \theta_a \le \pi$ and longitude $0 \le \phi_a < 2\pi$, as shown in Fig. 15. The longitudinal position, ϕ, on the sphere gives the orientation of the mode superposition. It is related to the azimuthal phase of the OAM mode via $\phi = 2\ell\varphi$, where φ is the azimuthal coordinate in real space for a

Figure 15

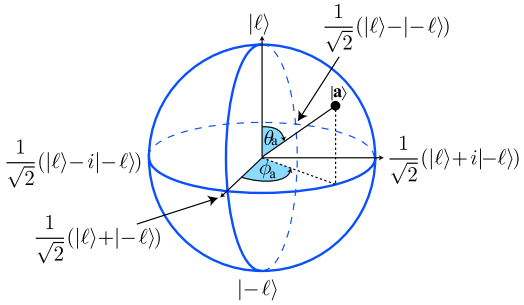

Bloch sphere for OAM states. The pure state $|\mathbf{a}\rangle$ is defined by its latitude ($0 \le \theta_a \le \pi$) and longitude ($0 \le \phi_a < 2\pi$) on the sphere. The poles ($\theta_a = 0, \pi$) represent the states $|\ell\rangle$, $|-\ell\rangle$ respectively, while around the equator ($\theta_a = \pi/2$) are the equally weighted superpositions of $|\ell\rangle$ and $|-\ell\rangle$ with no net OAM.

Laguerre–Gaussian mode. Hence the states $|\ell\rangle, |-\ell\rangle$ are represented by the poles of the sphere ($\theta_a = 0, \pi$), respectively, while equally weighted superpositions of $|\ell\rangle$ and $|-\ell\rangle$ correspond to points around the equator ($\theta_a = \pi/2$), with the equatorial position determined by the phase term, ϕ_a, between the two states.

For polarization, the action of a wave plate is modeled as a rotation of this vector about an axis corresponding to the orientation of the wave plate's optic axis and through an angle that depends on the retardation of the wave plate (e.g., 180° for a $\lambda/2$ plate and 90° for a $\lambda/4$ plate). For OAM states exactly the same transformations are performed by the cylindrical lens mode converters.

For *LG* modes with $\ell > 1$ the situation is more complicated. For modes of order N, i.e., all modes with the same Gouy phase, $(2p + \ell + 1) = N$, the number of orthogonal modes is $N + 1$ and $\ell_{\max} = N$. Therefore, the equivalent Poincaré sphere can only represent a two-dimensional subspace, most usually with the $p = 0$, $\ell = \pm N$ modes at the north and south poles, respectively, which sum to give a $2N$-fold rotationally symmetric "petal" mode at the equator.

For cases where a full representation of the modal set is required, then, although the equivalent to the Poincaré sphere is limited to two dimensions, the equivalent to the Jones matrices is not. Each mode is then represented by an $N + 1$ dimensional column vector, and the optical operations, such as mode converters and beam rotations, by $(N + 1) \times (N + 1)$ matrices [96].

As we have discussed, the OAM equivalent to birefringence is a phase shift between the *HG* modes of the same mode order N. However, within polarization we are also familiar with the concept of optical activity that introduces a phase shift between the circular polarization states (polar) and a corresponding rotation of the linear states (equatorial). However, optically active media do not interact with the OAM [97]. With reference to the Poincaré sphere equivalent, a relative phase shift, $\Delta\phi$, between the $\pm\ell$ polar states gives a rotation of the equatorial mode by $\Delta\theta = \Delta\phi/2\ell$, i.e., a rotation of the mode.

Moving away from defined laser modes toward general images, one recognizes that any image can be synthesized from the appropriate superposition of modes that form a complete basis set, e.g., *LG* modes. One notes that, for a given phase shift, the rotation of the modes scales as $1/\ell$ which, since the phase shift itself scales with ℓ, means that all modes rotate at the same rate and the image integrity is maintained—as is indeed observed when viewing an image through a Dove prism [98].

4.2. Rotational Doppler Shift

The Doppler shift is a familiar concept within waves of all types. If the velocity between source and receiver is v, then the light emitted from a moving source undergoes a frequency shift given by $\Delta\omega = \pm\omega_0 v/c$, positive when the source and the receiver are moving away from each other. In the 1970s Garetz noted that for circularly polarized light there was an analogous frequency shift for rotational motion between source and observer given as $\Delta\omega = \pm\sigma\omega$ [99,100], the sign depending on the relative rotational motion, where ω is the angular velocity and $\sigma = \pm 1$ for right- and left-handed polarized light, respectively. In his case he introduced a rotation in the optical beam by transmission through a pair of $\lambda/2$ plates. Spinning one of them with respect to the other causes the polarization state of the beam itself to be rotated at twice the speed of the wave plate. This frequency shift is akin to changing the frequency of a clock by rotating it so that the second hand moves around more quickly!

By analogy, one might expect a similar behavior for OAM, and indeed one sees immediately that a single rotation of a helically phased beam advances or retards the field by ℓ cycles. The corresponding frequency shift is given as $\Delta\omega = \ell\Omega$ [101], where ω is the frequency of the beam and Ω is the angular velocity between source and observer. Experimentally this is obtained not by $\lambda/2$ plates but by rotating mode converters either in the form of cylindrical lenses or, more conveniently, Dove prisms [65]. For a beam comprising a superposition of modes with different ℓ the result is multiple-frequency sidebands, which could, in principle, be used to deduce the OAM spectrum. This has potential applications for communication systems at either the classical [102] or quantum [103] level. When represented on the surface of the Poincaré sphere, and its OAM equivalent, one can interpret the rotational frequency shift for both SAM and OAM as examples of an evolving geometrical, or Berry, phase [94]. For a fixed orientation, α, of the Dove prisms, the geometrical phase shift is given by $\Delta\phi = 2\sigma\alpha$ and $\Delta\phi = 2\ell\alpha$, respectively.

Perhaps the most interesting aspect of these rotational frequency shifts is what happens when the beam contains both SAM and OAM, i.e., when it is both circularly polarized and helically phased. Plotting the vectorial nature of the field cross section of such beams reveals an $(\ell + \sigma)$-fold rotational symmetry. It follows that a single rotation of the beam around the beam axis changes the phase by $(\ell + \sigma)$ cycles, and hence for a spinning beam the rotational frequency shift is $\Delta\omega = (\ell + \sigma)\Omega$ [102]. For example, a beam with $\ell = 3$ and $\sigma = -1$ exhibits the same rotational frequency shift as a beam with $\ell = 1$ and $\sigma = 1$. This is one of the few examples of where the SAM and the OAM components act equivalently such that it is the total angular momentum that is of prime importance.

4.3. Mechanical Faraday Effect and Image Drag

Another area in which transformations for polarization and helical phase turn out to be completely equivalent is that of photon drag. In the 1970s Jones and his colleagues studied in great detail the transformations of light beams induced by moving media. Two effects are of note. First, when light is transmitted through a spinning window, he predicted, and confirmed, that the plane of polarization is rotated through a small angle given by $\Delta\theta_{pol} = \Omega(n_g - 1/n_\phi)L/c$, where Ω is the angular velocity of the dielectric medium, L is its length, and n_g and n_ϕ are the refractive indices corresponding to the group and phase velocities, respectively, of the light in the medium [104,105]; this is now known as the "mechanical Faraday effect" [106]. Second, when a beam of light is transmitted through a translating window it is displaced in the direction of motion of the window by an amount $\Delta x = v(n_g - 1/n_\phi)L/c$, where v is the translational velocity of the window [107]. For a rotating medium we may consider the transverse velocity of the medium to arise from the tangential component of the rotary motion of a glass rod, coaxial with the axis of the light beam ($v = \Omega r$, $\Delta x = r\Delta\theta$). If an image is considered to be made up of a number of such light beams, we can conclude that it will be rotated through the angle $\Delta\theta_{imag} = \Omega(n_g - 1/n_\phi)L/c$. Hence, a spinning window rotates both the polarization and the image through the same angle, as shown in Fig. 16, which can be interpreted as the equivalence of spin and OAM [108]. To date this image rotation has proved too difficult to observe; however, an equivalent experiment has been performed by viewing a rotating image through a stationary window yielding the anticipated result, albeit one that is complicated by the transformation in the rest frame [109].

5. Orbital Angular Momentum in Nonlinear and Quantum Optics

5.1. Optical Vortices and Orbital Angular Momentum in Kerr Media

The study of optical vortices in nonlinear media slightly predates the recognition of OAM. Nonlinear optical vortices were introduced by Coullet and collaborators when studying a Ginzburg–Landau equation for laser action [26]. It was then realized that for lasers with curved mirrors, optical vortices (or phase singularities) could be found in simple static [22] or dynamic [23] combinations of Laguerre–Gauss modes, the natural basis of transverse laser modes [25]. Optical vortices (otherwise known as spiral waves) can also form crystals and perform chaotic motion, such as that shown in Fig. 17, by pure transverse confinement in laser models [110] in a way similar to that of vortices in Bose–Einstein condensates [111].

A Kerr medium is one in which the refractive index varies with the incident intensity. This can lead to self-focusing or self-defocusing, depending on whether an increase in intensity increases or reduces the refractive index. The annular intensity of an OAM beam can

Figure 16

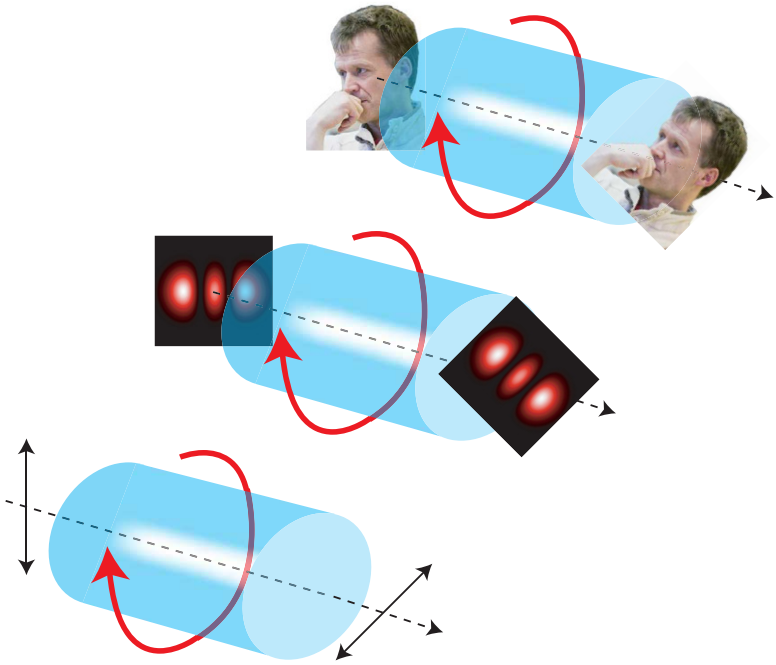

The mechanically induced ether drag associated with a spinning cylinder rotates both the polarization and the image through the same angle.

Figure 17

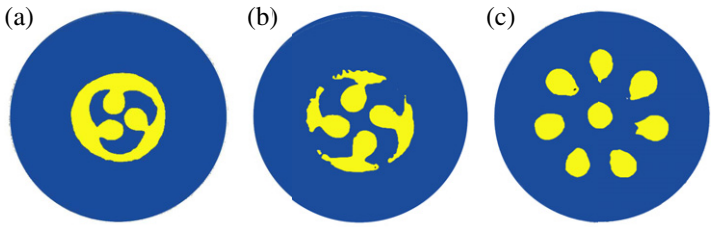

Behavior of spiral waves in lasers [110]. Spatial distribution of field in the presence of (a) three and (b) five spiral defects; yellow corresponds to low intensity, and blue to high intensity. Each phase singularity rotates around its core, while the whole pattern rotates around the center. (c) Spatial distribution of field with a total topological charge of 8. Seven defects rotate around a central defect.

therefore induce a column of high-refractive-index material along which a secondary beam can be guided [112]. Even without a secondary beam, asymmetry in the system may cause the annular ring to distort and the self-focusing to favor "hot spots," causing the beam to break up into individual transverse solitons. In this situation the original OAM behaves more like a series of inclined plane waves, causing the solitons to move tangentially with respect to the original ring, thereby conserving angular momentum [113,114]. Solitons and similar features have proved

Figure 18

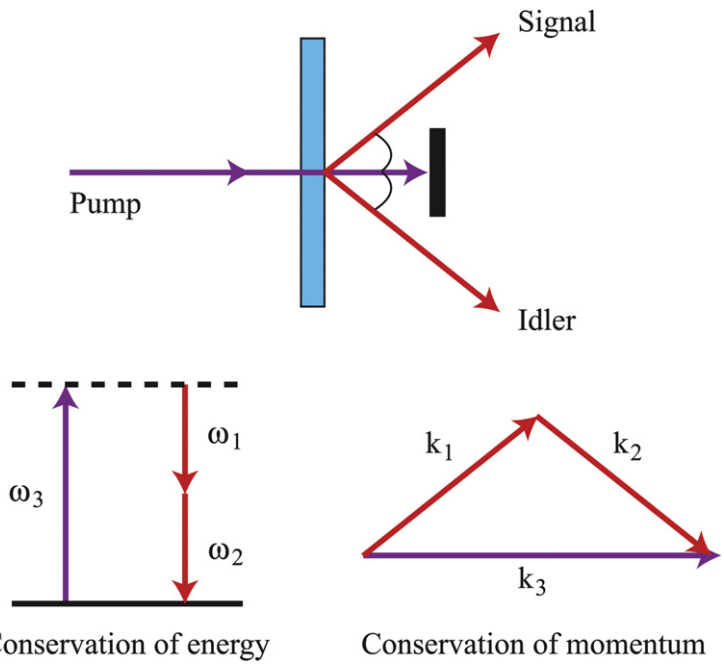

Conservation of energy and momentum in spontaneous parametric downconversion.

a rich area in which optical vortices and the OAM of light have led to new insights [115].

5.2. Second-Order Nonlinear Interactions

Second-order nonlinear interactions involve three waves: two low-frequency waves (1, 2) combine to exchange energy with a third wave (3) of higher frequency. Unsurprisingly, the conservation of energy within the optical fields sets the relationship between the three frequencies as $\omega_1 + \omega_2 = \omega_3$. The process is much more efficient when momentum within the optical fields is also conserved, i.e., $\mathbf{k_1} + \mathbf{k_2} = \mathbf{k_3}$, where $|\mathbf{k}| = \omega n(\omega)/c$ (Fig. 18). This momentum conservation is made much more complicated by the fact that the refractive index is itself a function of the frequency. Within nonlinear optics this latter requirement is called "phase matching," since the direction of energy flow between the low-frequency and the high-frequency waves depends on their relative phase.

Early experiments involving OAM in second-order nonlinear optics were on frequency doubling, where $2\omega_1 = 2\omega_2 = \omega_3$. For further simplicity, fields 1 and 2 are usually a single laser beam; e.g., a single infrared laser beam at 1064 nm incident on a nonlinear crystal such as KTP can be frequency doubled into the green at 532 nm. The KTP is birefringent, and by setting the incident angle appropriately it is possible to achieve phase matching. In a simplistic photon picture, two infrared photons combine to form a green one. The original motivation behind the investigation for the role that OAM may play in this process was

that, since the Poynting and momentum ($\mathbf{k}$) vectors have azimuthal components around the beam axis, it was thought that this might change (maybe preferentially) the phase-matching conditions. However, this proved not to be the case; rather, the phase-matching conditions for the helically phased incident beam were found to be identical to those for a plane wave [116]. It transpires that this is a result of the conservation of OAM within the optical fields, which is perhaps slightly surprising since, in general, the SAM is not conserved in the optical fields (it is usually transferred to the birefringent crystal). Conservation of OAM in the frequency-doubling process is simply stated as $\ell_1 + \ell_2 = \ell_3$. One also observes that, since the skew angle of the Poynting vector in a helically phased beam is $\ell/(kr)\hat{\boldsymbol{\phi}}$, where $\hat{\boldsymbol{\phi}}$ is a unit vector in the azimuthal direction [5], then in the case of frequency doubling, the doubling of the ℓ value is a requirement of the Poynting vector's keeping the same direction. For the multiple-ringed, $p > 0$, modes the situation is more complicated. The difference in the intensities of the rings is accentuated by the frequency-doubling process (the efficiency of which is proportional to the intensity), and thus the doubled mode is no longer a pure *LG* mode, but is rather a superposition of modes with different p but the same ℓ [117]. This difference in mode order in the resulting superposition means a difference in Gouy phase such that the superposition changes form upon propagation. However, none of these complications degrade the conservation of OAM within the optical fields. Similar conservation of OAM occurs in the more general case of sum-frequency mixing where $\omega_1 \neq \omega_2$ [118].

5.3. Parametric Down Conversion with OAM Beams

Depending on the relative phase of the three interacting waves, it is also possible to transfer the energy from the high-frequency wave to generate two lower-frequency waves (Fig. 20). This is called "parametric downconversion." In this situation the outcome is less constrained in that, from the conservation of energy, ω_1 and ω_2 may take a range of different values so long as they sum to give ω_3. The same flexibility exists for the momenta $\mathbf{k_1}$ and $\mathbf{k_2}$, too, and, since the OAM arises from the azimuthal component of $\mathbf{k}$, it follows that ℓ_1 and ℓ_2 are similarly flexible [48]. This is not a surprise since, for an extended incident beam, the output beam arising from parametric downconversion has only a limited spatial coherence and therefore can be expressed as an incoherent sum of different spatial modes. In essence, the conservation of OAM tells us that the output beams 1 and 2, although spatially incoherent, are coherent with respect to each other, thus leading to the entanglement of spatial modes [119].

Well-defined downconverted spatial modes can be achieved in stimulated parametric downconversion [120] or in optical parametric oscillators [121]. The stabilization of domain walls has been investigated in a degenerate, type-I optical parametric oscillator pumped with a cw *LG* mode [122]. A pump $LG_{0\ell}$ was shown to have a stable signal with phase profile $\exp(i\ell\phi/2)$. For even ℓ the number of domain walls trapped in the output signal is either zero or an even number. For odd ℓ the output is in a discontinuous state with fractional angular momentum.

Figure 19

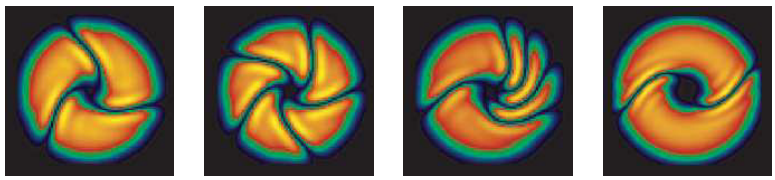

(a) (b) (c) (d)

Optical sprinklers: signals with a number of domain walls that rotate in time. (a)–(c) are for $\ell = 1$; (d) is for $\ell = 2$.

This ill-defined phase induces one (or an odd number of) domain wall with vanishing intensity in the radial direction, as shown in Fig. 19. This state is unusual in that it is a mode with fractional OAM given by the non-integer azimuthal index $\ell/2$ for ℓ odd.

5.4. Quantum Entanglement of Orbital Angular Momentum

Parametric downconversion sources play a central role in experiments to both show and apply the phenomenon of quantum entanglement. The downconverted photons 1 and 2 are generated through a process that conserves energy, momentum, angular momentum, etc. Therefore, measuring one of these parameters for one of the photons gives information about the same parameter of the other photon even though the photons may, at the time of measurement, be highly separated from each other. Such nonlocal correlations seem to follow naturally from conservation but lead directly to the Einstein, Podolosky, Rosen (EPR) paradox [123]. For example, it appears that strong correlations should exist both for measurements of position (i.e., both photons were generated at the same lateral position) and momentum (i.e., the momenta of 1 and 2 sum to give the momentum of 3). However, if one considers the case when the choice of whether to measure the momentum or position of the first photon is not made until the last possible moment, it follows that the second photon needs to be generated simultaneously with both a precise position and momentum, in conflict with the uncertainty principle. The EPR argument concludes that quantum mechanics is either incomplete or nonlocal, and this has been demonstrated by using a wide range of variables including, position–momentum [124] and time–energy [125].

It follows from these previous examples that strong correlations in OAM alone are not sufficient to demonstrate the EPR paradox. One has to show that one also obtains strong correlations in a complimentary basis. For OAM this was originally performed for specific superpositions of states, obtained when one deliberately slightly displaces one of the forked diffraction gratings transversely from the beam axis [126]. It was observed that the strength of the correlation depended on both the extent of the displacement and its direction—i.e., on both the magnitude and the relative phase of the modes in the superposition. This dependence on phase is exactly as required by quantum mechanics. Other modal superpositions have also been tested, including those

Figure 20

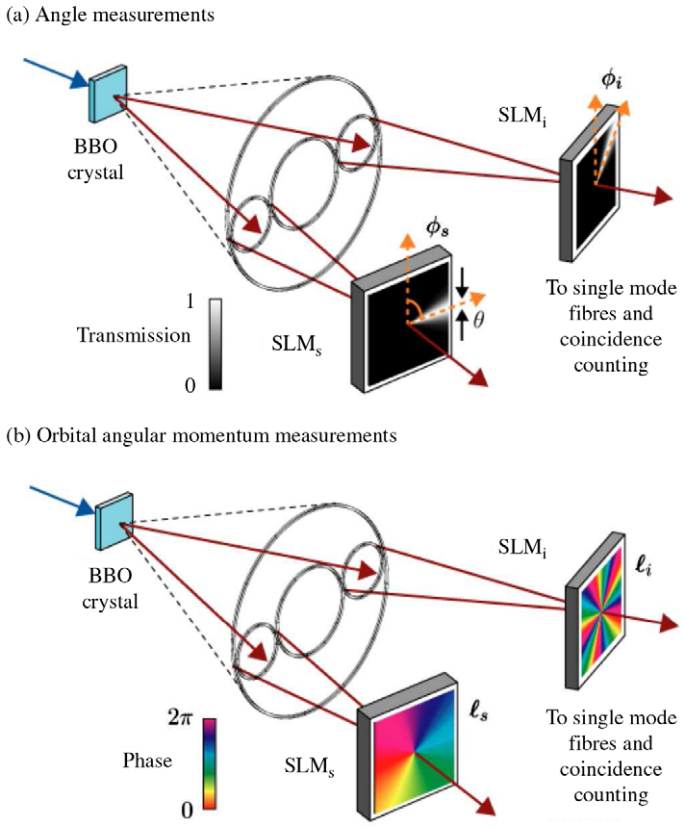

Spontaneous parametric downconversion produces entangled photons.

required in order to form helically phased modes but where the phase step is half-integer [127]. This breaks the rotational symmetry of the mode, leading to an angular sensitivity in the strength of the correlations. Most recently, by using wedge-shaped apertures, it has been possible to show strong correlations in angle that, when combined with correlations of OAM, illustrate a complete angle/angular momentum version of the original EPR paradox [128].

We described the EPR paradox as showing that quantum mechanics was either incomplete (i.e., possesses hidden variables) or nonlocal (i.e., measurement at one point can define the wavefunction over all space). The possibility of hidden variables (i.e., quantities that exist but cannot be measured) can be largely discounted through testing of Bell's [129] or other similar inequalities. The Bell's inequalities were famously violated in the 1980s for correlations in polarization [130], but can also be tested in any two-dimensional space. As we discussed in Subsection 4.1, the two-state space of polarization and its associated SAM can be represented on the surface of a Poincaré sphere. It is not surprising, therefore, that the Poincaré sphere equivalent for OAM has been used to formulate the Bell argument for OAM and that it too has been shown to violate the inequality, similarly discounting the hidden-variable theory [131].

One application of quantum entanglement is quantum cryptography, in which the presence of an eavesdropper is always revealed. The interest in using OAM for this purpose is that it represents a high-dimensional state space, meaning that each photon can be encoded to carry much larger amounts of information than if one were using polarization alone [132,133].

5.5. Logic Operations with Orbital Angular Momentum

One interesting opportunity for light carrying OAM, particularly at the single photon level, is its use in logic operations. OAM offers a multistate system that can be combined with SAM or other degrees of freedom. At a quantum level this may take the form of hyperentanglement, which is simultaneous entanglement within different variables [134], or hybrid entanglement, which is entanglement between different variables [135,136].

Key to more complicated logical operations are gates that allow the value of one variable to switch that of another, e.g., a CNOT gate, which has been implemented for OAM states [137]. One component of significance is the so-called q-plate [138], which sets the OAM of the transmitted light at one of two values depending on the sense of incident circular polarization. It is based on using liquid crystal to create a $\lambda/2$ plate whose optic axis rotates as a function of azimuthal position. The transmitted beam undergoes a geometric phase shift proportional to the angular position in the input beam such that the output beam has helical phase fronts [139,140]. This transformation between SAM and OAM using q-plates has been applied to quantum protocols such as quantum cloning [141]. Most recently it was shown that liquid crystal droplets held in optical tweezers could act as tiny components exchanging the angular momentum between spin and orbital components [142].

6. Measuring the Orbital Angular Momentum of Light

6.1. Forked Diffraction Gratings to Measure Orbital Angular Momentum

As we discussed in Subsection 2.3, the generation of helically phased beams carrying OAM is widely performed by using a forked diffraction grating which, when illuminated by a plane wave Gaussian beam, produces a helically phased beam in the first diffraction order. The process also works in reverse: a beam carrying an OAM of ℓ illuminating a forked diffraction grating with $-\ell$ produces a plane wave Gaussian beam, as in Fig. 21(top).

One way to ensure that the illuminating beam is a pure single-mode one is to couple the laser light through a single-mode fiber, collimating the output to illuminate the grating. Replacing the laser with a detector transforms the same grating system into a mode *detector*—the target mode is converted into a Gaussian mode, which is the only mode that couples efficiently into the fiber and detector (Fig. 21, bottom). If the

Figure 21

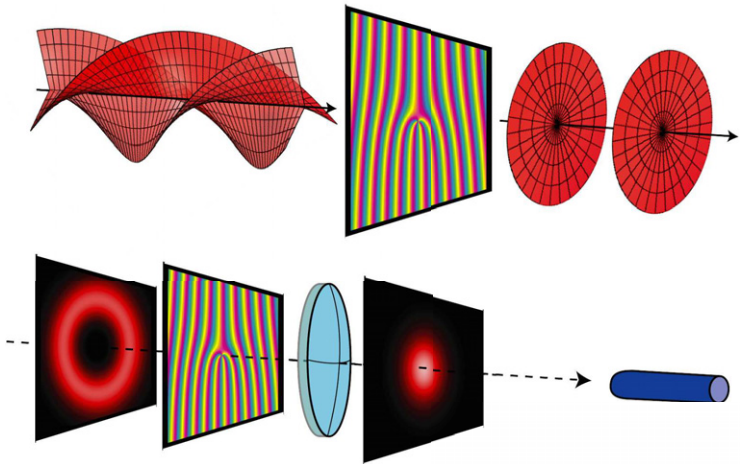

A diffractive optical element comprising a diffraction grating with fork dislocation centered on the beam axis can convert a helically phased mode into the fundamental Gaussian mode, which can then be coupled to single-mode fiber.

detector is a high-quality photomultiplier or avalanche photodiode, then modes, or complex superpositions of modes, can be measured even at the level of single photons, and this has been used in various experiments of the quantum entanglement of OAM [126]. However, all such holograms can measure only one mode at a time, and if a large state space (as in the case of OAM) is to be measured, one must test for each of the modes in turn. It follows that the efficiency of such an approach can never exceed $1/N$, where N is the number of modes to be assessed. This limit in efficiency negates many of the potential advantages that the large state space of OAM may have offered. More complicated holograms can be designed where different input modes produce Gaussian beams in different angular orders [143–145]; however, in all of these the incident energy is still split between the outputs, leading again to an approximate $1/N$ limit in efficiency.

6.2. Measuring OAM by Interferometry

In the early work on generation of optical vortices it was noted that when a helically phased beam is interfered with a plane wave it produces a spiral interference pattern with ℓ fringes [146–148]. However, using such a system as a measurement device, of course, depends on having many photons in the same state and hence cannot be applied to single-photon measurement.

In principle, the frequency sideband induced by the rotational frequency shift could be used to measure ℓ [102] (see Subsection 4.2). However, the perfect rotation of a beam is not so straightforward, and it is difficult to isolate the effects of rotation from those arising from slight misalignment [149]. In fact it is easier to use a static approach in which Dove prisms are introduced into each arm of an interferometer. If the

angle between the prisms is $\Delta\alpha$ then the phase shift between the arms is given by $\Delta\phi = 2\ell\Delta\alpha$. If $\Delta\alpha = \pi/2$, then all inputs with even values of ℓ will constructively interfere at one output port, and all those with odd values of ℓ will constructively interfere at the other output. A system such as this is able to sort odd and even values of ℓ even at the level of single photons. Cascading additional interferometers with different values of $\Delta\alpha$ allows the modes to be further sorted, in principle N different states requiring $N-1$ interferometers [150]. Such a system was shown for four states but to date has proved too challenging to engineer for more states and "turnkey" operation.

Finally, it is also possible to introduce additional wave plates into the interferometers such that, similar to the rotational frequency shift, they sort on the basis of the total angular momentum rather than the OAM or SAM alone [151].

6.3. Orbital Angular Momentum and Diffraction by Apertures and Angular Uncertainty

Changing the phase structure of a beam modifies the diffraction pattern produced by a subsequent aperture. For example, inclining a plane wave prior to a diffraction grating translates the diffraction pattern. This naturally leads to the question as to what happens when a diffraction grating is illuminated with an *LG* beam. In the case of a single edge, the azimuthal component to the momentum of an *LG* beam results in a rotation of the light in the far field, with the direction depending upon the sign of ℓ [152]. For the cases of a single slit and Young's double slits, it has been observed that the helical nature of the phase front gives rise to a displacement of the fringes that changes with vertical position, thereby introducing a slight dogleg into the otherwise straight fringes. The sense of the dogleg depends upon the sign of ℓ [153,154]. More complex diffraction gratings, e.g., arrays of pinholes, give rise to more complicated diffraction patterns, and again it is possible to recognize the incident value of ℓ from the patterns that result [155]. One fascinating example is the diffraction of an *LG* beam by a triangular aperture. The result is a triangular array of diffracted spots containing $\sum_{i=1}^{\ell+1} i = (\ell+1)(\ell+2)/2$ local maxima, oriented at right angles to the aperture with a sense that depends on the sign of ℓ [156]. The value of ℓ is also directly related to external points of the lattice forming a triangle: $\ell = N-1$, where N is the number of points on any side of the triangle. However, all of these variants require many photons in the same state in order to form the characteristic fringe pattern and hence cannot be used to measure the ℓ of single photons.

An aperture of particular interest is one that either transmits or blocks an angular sector of the beam. The relationship between the expression of a field in terms of its OAM spectrum and an equivalent expression in terms of its angular distribution is one of a Fourier series. One would expect that variables that are related to each other by Fourier transforms would lead to uncertainty relationships of the type typified by position and linear momentum. The famous Heisenberg uncertainty relationship states that the product of the variances $\Delta x\Delta p_x > \hbar/2$. OAM and angular position are also linked by a Fourier relationship [157];

Figure 22

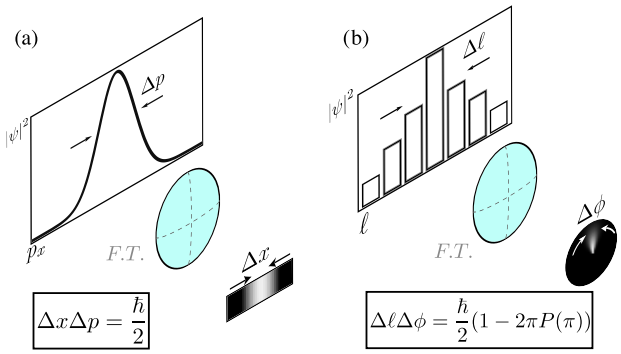

The uncertainty relationship for angle-angular momentum, analogous to that for position and momentum.

however, the situation is quite complicated. Unlike linear position, which is unbounded, angular position is periodic over the 2π range. This means that, if calculated as an integral between $\pm\infty$, its standard deviation is ill-defined. This 2π ambiguity has previously led to some debate as to the form by which the uncertainty relationship can be expressed for the angular variable [158]. However, if one restricts the calculation of variance to a single 2π range, one obtains a practical measure of angular uncertainty and can show that there exists a simple uncertainty relationship for angular momentum, namely, $\Delta\ell\Delta\phi > |1 - 2\pi P_\pi|/2$ [159]. This allows one to calculate the minimum spread in ℓ for an aperture function of angular width, $\Delta\phi$, as in Fig. 22. Such angular uncertainty relationships are also demonstrated at the single-photon level for demonstration of the angular equivalent to the EPR paradox mentioned above.

6.4. Measuring Orbital Angular Momentum by Image Reformatting

A recently reported approach to measuring OAM at, potentially, the single-photon level draws its inspiration from the ease with which plane waves can be distinguished from each other in direction space. If focused by a lens, each plane wave direction results in a bright spot in the focal plane of the lens, with its transverse Y position related to the angular direction of the incoming wave. Providing that the direction change amounts to at least an additional phase change of 2π across the beam, the separation of the spots corresponds to at least the Rayleigh resolution criterion. For measuring OAM, the key optical component required is one that transforms an azimuthal position in the input beam into a transverse position in the output beam, i.e., an optical element that transforms a helically phased beam into a transverse phase gradient. As the ℓ index is incremented by one, the azimuthal phase term changes by 2π. Such components have been studied previously [160,161] and use a shaped optical component to refract the incident rays such that concentric circles in the input plane are reformatted to parallel lines at the output. Unfortunately, the reformatting introduces a phase aberration

Figure 23

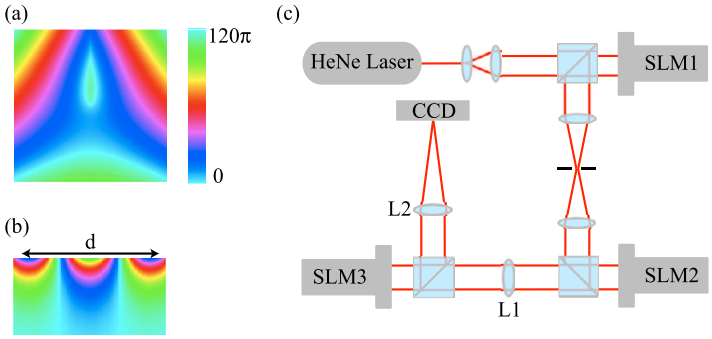

Phase profiles of (a) the transforming and (b) the phase-correcting optical element; d is the length of the transformed beam. In (b) only that part of the phase-correcting element is shown that is illuminated by the transformed beam. In the experiment, the phase profiles are displayed on the SLMs with 2% phase modulation. (c) Schematic overview of the setup. SLMs are used both to generate Laguerre–Gaussian beams (SLM1) and to create the desired phase profiles for the transforming and phase-correcting optical elements (SLM2 and SLM3, respectively). L1 is the Fourier-transforming lens, and lens L2 focuses the transformed beams. Beam splitters ensure perpendicular incidence on the SLMs.

that must be corrected in the output plane; i.e., an input plane wave must remain a plane wave. A demonstration system, shown in Fig. 23, has been built where the reformatter and phase corrector have been implemented on SLMs. After the phase corrector, a simple lens focuses each input mode to a specific lateral position where it can be recorded with a detector array [162]. The complete system has been demonstrated for the separation of 11 OAM states, with minimal cross-talk between channels. However, the quest for high efficiency requires that, in the future, the SLMs be replaced with real refractive components. Unlike the various apertures and holographic schemes we have discussed above, the image reformatter holds the potential to measure the ℓ of single photons and is far less technically demanding than the interferometric approach.

6.5. Use of Orbital Angular Momentum in Imaging

The detection of the OAM components of an image creates a route to contrast enhancement within different forms of imaging. For example, the position of phase singularities can be identified by using a forked hologram in the Fourier plane [46]. More complicated analysis of the orbital angular spectrum from a specific point can reveal the helicity of a surface or other phase gradients [163]. Many contrast enhancement techniques exist in the field of optical microscopy, ranging from dark-field and phase contrast to interference. Many of these are achieved by inserting a phase mask into the image train of a microscope. Rather than having dedicated phase masks for each imaging modality, most of them can be implemented by using an SLM as a diffractive optical component [164]. Of particular interest to us is

Figure 24

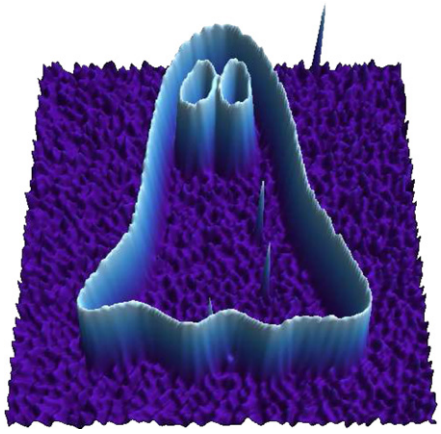

Ghost imaging: coincidence measurements of two beams of entangled photons—one of which interacts with an object and one of which doesn't—can be used to reconstruct a "ghost" image of the object.

when the phase mask corresponds to a spiral phase plate, effectively transforming the point spread function of the microscope into a helically phased ring. When viewing a phase object, regions of uniform phase result in destructive interference, whereas phase edges appear as bright lines—giving unidirectional edge enhancement. Changing the phase mask to introduce a plane wave reference gives an interferogram, but one where a surface curvature gives spiral fringes that are clockwise or anticlockwise depending on the sign of the curvature [165,166]. This last feature breaks the usual interferometric degeneracy associated with distinguishing up from down! Most recently, the same technique has been employed at the level of single photons within a ghost imaging arrangement where the phase filter is nonlocal with respect to the object [167], revealing in the images a violation of a Bell's inequality. The results are shown in Fig. 24.

When a highly localized object is viewed with a spiral phase plate, the resulting image is a single ring. Such an arrangement allows one to look for neighboring, but much less intense, sources [59]. As mentioned above in Subsection 2.5, one example of this problem is in astronomy, where one may wish to block light from a bright star so as to make orbiting planets more visible. Such applications of spiral phase plates are currently under investigation and trial [168,169].

Some thought has been given to the use of OAM in various other astronomical opportunities [170]. A promising option seems to be in the radio wave domain, where relative phase measurements over an array of detectors may reveal OAM in the signals from distant sources.

7. Reflections on the Contribution of and Future Opportunities for Orbital Angular Momentum

Although OAM for light had been recognized as a requirement for high-order transitions, the fact that OAM-carrying beams could be, and indeed had already been, made in the laboratory was a major contribution of Allen *et al.* [1]. Beyond the many high-class papers that OAM has inspired, it may transpire that OAM becomes the key to important applications in the micromanipulation, imaging, or communication systems that we have discussed. However, perhaps more important is that we could argue that OAM has taught us to think differently about light. The requirement to control both the phase and the intensity of light beams, often through the use of SLMs, has led to the study of other beam types in both the optical and the nonoptical regimes. OAM led to a vigorous interest in optical tweezers and new manifestations of quantum entanglement. Phenomenologically the OAM basis set has naturally led to a recognition of rotational frequency shifts, angular uncertainty relations, and Poincaré sphere equivalents for partial modes, all of which were possible in a rectangular basis but sufficiently obscure to have been missed before OAM. Whether OAM delivers the "killer application" we will have to wait and see, but it seems without doubt that its story is set to continue for some time.

Acknowledgments

This research was supported by the DARPA InPho program through the U.S. Army Research Office award W911NF-10-1-0395. We thank the UK's Engineering and Physical Sciences Research Council (EPSRC), and M. J. Padgett thanks the Royal Society and the Wolfson Foundation. We also thank Martin Lavery for a careful reading of the manuscript. Finally, we thank the Optics group at the University of Glagow and the CNQO group at the University of Strathclyde for many useful contributions.

References and Notes

1. L. Allen, M. W. Beijersbergen, R. J. C. Spreeuw, and J. P. Woerdman, "Orbital angular-momentum of light and the transformation of Laguerre–Gaussian laser modes," Phys. Rev. A **45**, 8185–8189 (1992).
2. L. Mandel and E. Wolf, *Optical Coherence and Quantum Optics* (Cambridge University Press, 1995).
3. L. Allen, M. Padgett, and M. Babiker, "The orbital angular momentum of light," Prog. Opt. **39**, 291–372 (1999).
4. J. W. Simmons and M. J. Guttmann, *States, Waves, and Photons: a Modern Introduction to Light* (Addison-Wesley, 1970).
5. M. J. Padgett and L. Allen, "The Poynting vector in Laguerre–Gaussian laser modes," Opt. Commun. **121**, 36–40 (1995).
6. J. Leach, S. Keen, M. J. Padgett, C. Saunter, and G. D. Love, "Direct measurement of the skew angle of the Poynting vector in a helically phased beam," Opt. Express **14**, 11919–11924 (2006).

7. S. Barnett and L. Allen, "Orbital angular momentum and non paraxial light beams," Opt. Commun. **110**, 670–678 (1994).
8. Y. Zhao, J. S. Edgar, G. D. M. Jeffries, D. McGloin, and D. T. Chiu, "Spin-to-orbital angular momentum conversion in a strongly focused optical beam," Phys. Rev. Lett. **99**, 073901 (2007).
9. T. A. Nieminen, A. B. Stilgoe, N. R. Heckenberg, and H. Rubinsztein-Dunlop, "Angular momentum of a strongly focused Gaussian beam," J. Opt. A. Pure Appl. Opt. **10**, 115005 (2008).
10. S. M. Barnett, "Optical angular-momentum flux," J. Opt. B Quantum Semiclass. Opt. **4**, 7–16 (2002).
11. J. Poynting, "The wave motion of a revolving shaft, and a suggestion as to the angular momentum in a beam of circularly polarised light," Proc. R. Soc. Lond. A Ser. A **82**, 560–567 (1909).
12. R. Beth, "Mechanical detection and measurement of the angular momentum of light," Phys. Rev. **50**, 115–125 (1936).
13. J. D. Jackson, *Classical Electrodynamics* 3rd ed. (Wiley, 1999).
14. P. Dirac, "Quantised singularities in the electromagnetic field," Proc. R. Soc. Lond. A **133**, 60–72 (1931).
15. J. F. Nye and M. Berry, "Dislocations in wave trains," Proc. R. Soc. Lond. A **336**, 165–190 (1974).
16. M. Berry, J. Nye, and F. Wright, "The elliptic umbilic diffraction catastrophe," Phil. Trans. R. Soc. Lond. **291**, 453–484 (1979).
17. J. M. Vaughan and D. Willetts, "Interference properties of a light-beam having a helical wave surface," Opt. Commun. **30**, 263–267 (1979).
18. C. Tamm, "Frequency locking of 2 transverse optical modes of a laser," Phys. Rev. A **38**, 5960–5963 (1988).
19. C. Tamm and C. Weiss, "Bistability and optical switching of spatial patterns in a laser," J. Opt. Soc. Am. B **7**, 1034–1038 (1990).
20. L. A. Lugiato, F. Prati, L. M. Narducci, and G.-L. Oppo, "Spontaneous breaking of the cylindrical symmetry in lasers," Opt. Commun. **69**, 387–392 (1989).
21. L. A. Lugiato, G.-L. Oppo, J. R. Tredicce, L. M. Narducci, and M. A. Pernigo, "Instability and spatial complexity in a laser," J. Opt. Soc. Am. B **7**, 1019–1033 (1990).
22. M. Brambilla, F. Battipiede, L. A. Lugiato, V. Penna, F. Prati, C. Tamm, and C. O. Weiss, "Transverse laser patterns. I. Phase singularity crystals," Phys. Rev. A **43**, 5090–5113 (1991).
23. M. Brambilla, M. Cattaneo, L. A. Lugiato, R. Pirovano, F. Prati, A. J. Kent, G.-L. Oppo, A. B. Coates, C. O. Weiss, C. Green, E. J. D'Angelo, and J. R. Tredicce, "Dynamical transverse laser patterns. I. Theory," Phys. Rev. A **49**, 1427–1451 (1994).
24. A. B. Coates, C. O. Weiss, C. Green, E. J. D'Angelo, J. R. Tredicce, M. Brambilla, M. Cattaneo, L. A. Lugiato, R. Pirovano, F. Prati, A. J. Kent, and G.-L. Oppo, "Dynamical transverse laser patterns. II. Experiments," Phys. Rev. A **49**, 1452–1466 (1994).
25. G. D'Alessandro and G.-L. Oppo, "Gauss–Laguerre modes: a sensible basis for laser dynamics," Opt. Commun. **88**, 130–136 (1992).
26. P. Coullet, G. Gil, and F. Rocca, "Optical vortices," Opt. Commun. **73**, 403–408 (1989).
27. V. Bazhenov, M. V. Vasnetsov, and M. S. Soskin, "Laser-beams with screw dislocations in their wave-fronts," JETP. Lett. **52**, 429–431 (1990).

28. M. V. Berry and M. R. Dennis, "Phase singularities in isotropic random waves," Proc. R. Soc. Lond. A **456**, 2059–2079 (2000).
29. J. Masajada and B. Dubik, "Optical vortex generation by three plane wave interference," Opt. Commun. **198**, 21–27 (2001).
30. K. O'Holleran, M. Padgett, and M. Dennis, "Topology of optical vortex lines formed by the interference of three, four, and five plane waves," Opt. Express **14**, 3039–3044 (2006).
31. J. F. Nye, *Natural Focusing and Fine Structure of Light: Caustics and Wave Dislocations* 1st ed. (Taylor & Francis, 1999).
32. K. O'Holleran, M. R. Dennis, F. Flossmann, and M. J. Padgett, "Fractality of light's darkness," Phys. Rev. Lett. **100**, 053902 (2008).
33. M. V. Berry and M. R. Dennis, "Knotted and linked phase singularities in monochromatic waves," Proc. R. Soc. Lond. A **457**, 2251–2263 (2001).
34. K. O'Holleran, M. Dennis, and M. Padgett, "Topology of light's darkness," Phys. Rev. Lett. **102**, 143902 (2009).
35. G. Molina-Terriza, J. P. Torres, and L. Torner, "Twisted photons," Nat. Phys. **3**, 305–310 (2007).
36. S. Franke-Arnold, L. Allen, and M. Padgett, "Advances in optical angular momentum," Laser Photon. Rev. **2**, 299–315 (2008).
37. M. W. Beijersbergen, R. Coerwinkel, M. Kristensen, and J. P. Woerdman, "Helical-wavefront laser beams produced with a spiral phaseplate," Opt. Commun. **112**, 321–327 (1994).
38. G. A. Turnbull, D. A. Roberson, G. M. Smith, L. Allen, and M. J. Padgett, "Generation of free-space Laguerre–Gaussian modes at millimetre-wave frequencies by use of a spiral phaseplate," Opt. Commun. **127**, 183–188 (1996).
39. S. Oemrawsingh, J. van Houwelingen, E. Eliel, J. P. Woerdman, E. Verstegen, J. Kloosterboer, and G. 't Hooft, "Production and characterization of spiral phase plates for optical wavelengths," Appl. Optics **43**, 688–694 (2004).
40. K. Sueda, G. Miyaji, N. Miyanaga, and M. Nakatsuka, "Laguerre–Gaussian beam generated with a multilevel spiral phase plate for high intensity laser pulses," Opt. Express **12**, 3548–3553 (2004).
41. A. E. Siegman, *Lasers* (University Science Books, 1986).
42. M. Kolobov ed., *Quantum Imaging* (Springer, 2007).
43. J. Durnin, J. J. Miceli Jr., and J. Eberly, "Diffraction-free beams," Phys. Rev. Lett. **58**, 1499–1501 (1987).
44. J. Gutiérrez-Vega, M. Iturbe-Castillo, and S. Chávez-Cerda, "Alternative formulation for invariant optical fields: Mathieu beams," Opt. Lett. **25**, 1493–1495 (2000).
45. V. Bazhenov, M. S. Soskin, and M. V. Vasnetsov, "Screw dislocations in light wavefronts," J. Mod. Opt. **39**, 985–990 (1992).
46. N. R. Heckenberg, R. McDuff, C. P. Smith, H. Rubinsztein-Dunlop, and M. Wegener, "Laser beams with phase singularities," Opt. Quantum. Electron **24**, S951–S962 (1992).
47. N. R. Heckenberg, R. McDuff, C. P. Smith, and A. White, "Generation of optical phase singularities by computer-generated holograms," Opt. Lett. **17**, 221–223 (1992).
48. J. Arlt, K. Dholakia, L. Allen, and M. J. Padgett, "Parametric downconversion for light beams possessing orbital angular momentum," Phys. Rev. A **59**, 3950–3952 (1999).

49. M. Dennis, K. O'Holleran, and M. Padgett, "Singular optics: optical vortices and polarization singularities," Prog. Opt. **53**, 293–363 (2009).
50. R. W. Gerchberg and W. Saxton, "Practical algorithm for determination of phase from image and diffraction plane pictures," Optik **35**, 237–246 (1972).
51. A. Jesacher, C. Maurer, A. Schwaighofer, S. Bernet, and M. Ritsch-Marte, "Near-perfect hologram reconstruction with a spatial light modulator," Opt. Express **16**, 2597–2603 (2008).
52. J. Kirk and A. Jones, "Phase-only complex-valued spatial filter," J. Opt. Soc. Am. **61**, 1023–1028 (1971).
53. J. Leach, M. R. Dennis, J. Courtial, and M. J. Padgett, "Vortex knots in light," New J. Phys. **7**, 55 (2005).
54. M. R. Dennis, R. P. King, B. Jack, K. O'Holleran, and M. J. Padgett, "Isolated optical vortex knots," Nat. Phys. **6**, 118–121 (2010).
55. B. Jack, A. M. Yao, J. Leach, J. Romero, S. Franke-Arnold, D. G. Ireland, S. M. Barnett, and M. J. Padgett, "Entanglement of arbitrary superpositions of modes within two-dimensional orbital angular momentum state spaces," Phys. Rev. A **81**, 043844 (2010).
56. M. W. Beijersbergen, L. Allen, H. van der Veen, and J. P. Woerdman, "Astigmatic laser mode converters and transfer of orbital angular momentum," Opt. Commun. **96**, 123–132 (1993).
57. N. González, G. Molina-Terriza, and J. Torres, "How a Dove prism transforms the orbital angular momentum of a light beam," Opt. Express **14**, 9093–9102 (2006).
58. G. A. Swartzlander and R. I. Hernandez-Aranda, "Optical Rankine vortex and anomalous circulation of light," Phys. Rev. Lett. **99**, 163901 (2007).
59. G. A. Swartzlander, "Peering into darkness with a vortex spatial filter," Opt. Lett. **26**, 497–499 (2001).
60. G. Foo, D. M. Palacios, and G. A. Swartzlander, "Optical vortex coronagraph," Opt. Lett. **30**, 3308–3310 (2005).
61. G. Gbur, T. Visser, and E. Wolf, "Anomalous behavior of spectra near phase singularities of focused waves," Phys. Rev. Lett. **88**, 013901 (2002).
62. M. V. Berry, "Coloured phase singularities," New J. Phys. **4**, 66 (2002).
63. M. V. Berry, "Exploring the colours of dark light," New J. Phys. **4**, 74 (2002).
64. J. Leach and M. Padgett, "Observation of chromatic effects near a white-light vortex," New J. Phys. **5**, 154 (2003).
65. J. Courtial, K. Dholakia, D. Robertson, L. Allen, and M. J. Padgett, "Measurement of the rotational frequency shift imparted to a rotating light beam possessing orbital angular momentum," Phys. Rev. Lett. **80**, 3217–3219 (1998).
66. B. Thidé, H. Then, J. Sjöholm, K. Palmer, J. Bergman, T. D. Carozzi, Y. N. Istomin, N. H. Ibragimov, and R. Khamitova, "Utilization of photon orbital angular momentum in the low-frequency radio domain," Phys. Rev. Lett. **99**, 087701 (2007).
67. S. Sasaki and I. Mcnulty, "Proposal for generating brilliant x-ray beams carrying orbital angular momentum," Phys. Rev. Lett. **100**, 124801 (2008).
68. M. Uchida and A. Tonomura, "Generation of electron beams carrying orbital angular momentum," Nature **464**, 737–739 (2010).
69. H. T. J. Verbeeck and P. Schattschneider, "Production and application of electron vortex beams," Nature **467**, 301–304 (2010).

70. K. Volke-Sepúlveda, A. O. Santillán, and R. R. Boullosa, "Transfer of angular momentum to matter from acoustical vortices in free space," Phys. Rev. Lett. **100**, 024302 (2008).
71. K. D. Skeldon, C. Wilson, M. Edgar, and M. J. Padgett, "An acoustic spanner and its associated rotational doppler shift," New J. Phys. **10**, 013018 (2008).
72. H. He, M. Friese, N. R. Heckenberg, and H. Rubinsztein-Dunlop, "Direct observation of transfer of angular momentum to absorptive particles from a laser beam with a phase singularity," Phys. Rev. Lett. **75**, 826–829 (1995).
73. N. Simpson, K. Dholakia, L. Allen, and M. Padgett, "Mechanical equivalence of spin and orbital angular momentum of light: an optical spanner," Opt. Lett. **22**, 52–54 (1997).
74. D. Grier, "A revolution in optical manipulation," Nature **424**, 810–816 (2003).
75. M. Padgett and L. Allen, "Optical tweezers and spanners," Phys. World **10**, 35–38 (1997).
76. M. Friese, T. Nieminen, N. R. Heckenberg, and H. Rubinsztein-Dunlop, "Optical alignment and spinning of laser-trapped microscopic particles," Nature **394**, 348–350 (1998).
77. A. O'Neil, I. MacVicar, L. Allen, and M. Padgett, "Intrinsic and extrinsic nature of the orbital angular momentum of a light beam," Phys. Rev. Lett. **88**, 053601 (2002).
78. L. Paterson, M. MacDonald, J. Arlt, W. Sibbett, P. Bryant, and K. Dholakia, "Controlled rotation of optically trapped microscopic particles," Science **292**, 912 (2001).
79. H. Luo, Z. Ren, W. Shu, and S. Wen, "Reversed propagation dynamics of Laguerre–Gaussian beams in left-handed materials," Phys. Rev. A **77**, 023812 (2008).
80. J. Courtial and M. Padgett, "Limit to the orbital angular momentum per unit energy in a light beam that can be focused onto a small particle," Opt. Commun. **173**, 269–274 (2000).
81. E. Higurashi, H. Ukita, H. Tanaka, and O. Ohguchi, "Optically induced rotation of anisotropic micro-objects fabricated by surface micromachining," Appl. Phys. Lett. **64**, 2209–2210 (1994).
82. M. Friese, H. Rubinsztein-Dunlop, J. Gold, P. Hagberg, and D. Hanstorp, "Optically driven micromachine elements," Appl. Phys. Lett. **78**, 547–549 (2001).
83. G. Knoner, S. Parkin, T. A. Nieminen, V. L. Y. Loke, N. R. Heckenberg, and H. Rubinsztein-Dunlop, "Integrated optomechanical microelements," Opt. Express **15**, 5521–5530 (2007).
84. K. Ladavac and D. Grier, "Micro-optomechanical pumps assembled and driven by holographic optical vortex arrays," Opt. Express **12**, 1144–1149 (2004).
85. J. Leach, H. Mushfique, R. di Leonardo, M. Padgett, and J. Cooper, "An optically driven pump for microfluidics," Lab Chip **6**, 735–739 (2006).
86. M. Babiker, W. L. Power, and L. Allen, "Light-induced torque on moving atoms," Phys. Rev. Lett. **73**, 1239–1242 (1994).
87. L. Allen, M. Babiker, and W. L. Power, "Azimuthal Dopper-shift in light-beams with orbital angular momentum," Opt. Commun. **112**, 141–144 (1994).

88. T. Kuga, Y. Torii, N. Shiokawa, T. Hirano, Y. Shimizu, and H. Sasada, "Novel optical trap of atoms with a doughnut beam," Phys. Rev. Lett. **78**, 4713–4716 (1997).
89. J. Arlt, T. Hitomi, and K. Dholakia, "Atom guiding along Laguerre–Gaussian and Bessel light beams," Appl. Phys. B: Lasers and Optics **71**, 549–554 (2000).
90. K. Gahagan and G. A. Swartzlander, "Optical vortex trapping of particles," Opt. Lett. **21**, 827–829 (1996).
91. M. F. Andersen, C. Ryu, P. Clade, V. Natarajan, A. Vaziri, K. Helmerson, and W. D. Phillips, "Quantized rotation of atoms from photons with orbital angular momentum," Phys. Rev. Lett. **97**, 170406 (2006).
92. R. Pugatch, M. Shuker, O. Firstenberg, A. Ron, and N. Davidson, "Topological stability of stored optical vortices," Phys. Rev. Lett. **98**, 203601 (2007).
93. D. Sanvitto, F. M. Marchetti, M. H. Szymańska, G. Tosi, M. Baudisch, F. P. Laussy, D. N. Krizhanovskii, M. S. Skolnick, L. Marrucci, A. Lemaître, J. Bloch, C. Tejedor, and L. Viña, "Persistent currents and quantized vortices in a polariton superfluid," Nat. Phys. **6**, 527–533 (2010).
94. M. J. Padgett and J. Courtial, "Poincare-sphere equivalent for light beams containing orbital angular momentum," Opt. Lett. **24**, 430–432 (1999).
95. E. Galvez, P. Crawford, H. Sztul, M. Pysher, P. Haglin, and R. Williams, "Geometric phase associated with mode transformations of optical beams bearing orbital angular momentum," Phys. Rev. Lett. **90**, 203901 (2003).
96. L. Allen, J. Courtial, and M. Padgett, "Matrix formulation for the propagation of light beams with orbital and spin angular momenta," Phys. Rev. E **60**, 7497–7503 (1999).
97. F. Araoka, T. Verbiest, K. Clays, and A. Persoons, "Interactions of twisted light with chiral molecules: an experimental investigation," Phys. Rev. A **71**, 055401 (2005).
98. L. Allen and M. Padgett, "Equivalent geometric transformations for spin and orbital angular momentum of light," J. Mod. Opt. **54**, 487–491 (2007).
99. B. Garetz and S. Arnold, "Variable frequency-shifting of circularly polarized laser-radiation via a rotating half-wave retardation plate," Opt. Commun. **31**, 1–3 (1979).
100. B. Garetz, "Angular Dopper effect," J. Opt. Soc. Am. **71**, 609–611 (1981).
101. G. Nienhuis, "Doppler effect induced by rotating lenses," Opt. Commun. **132**, 8–14 (1996).
102. J. Courtial, D. Robertson, K. Dholakia, L. Allen, and M. Padgett, "Rotational frequency shift of a light beam," Phys. Rev. Lett. **81**, 4828–4830 (1998).
103. G. Molina-Terriza, J. Torres, and L. Torner, "Management of the angular momentum of light: preparation of photons in multidimensional vector states of angular momentum," Phys. Rev. Lett. **88**, 013601 (2001).
104. R. V. Jones, "Rotary 'aether drag'," Proc. R. Soc. Lond. A **349**, 423–439 (1976).
105. M. A. Player, "On the dragging of the plane of polarization of light propagating in a rotating medium," Proc. R. Soc. Lond. A **349**, 441–445 (1976).
106. G. Nienhuis, J. P. Woerdman, and I. Kuscer, "Magnetic and mechanical Faraday effects," Phys. Rev. A **46**, 7079–7092 (1992).
107. R. V. Jones, "'Fresnel aether drag' in a transversely moving medium," Proc. R. Soc. Lond. A **328**, 337–352 (1972).

108. M. Padgett, G. Whyte, J. Girkin, A. Wright, L. Allen, P. Ohberg, and S. M. Barnett, "Polarization and image rotation induced by a rotating dielectric rod: an optical angular momentum interpretation," Opt. Lett. **31**, 2205–2207 (2006).
109. J. Leach, A. J. Wright, J. B. Gotte, J. M. Girkin, L. Allen, S. Franke-Arnold, S. M. Barnett, and M. J. Padgett, "'Aether drag' and moving images," Phys. Rev. Lett. **100**, 153902 (2008).
110. L. Gil, K. Emilsson, and G.-L. Oppo, "Dynamics of spiral waves in a spatially inhomogenous Hopf bifurcation," Phys. Rev. A **45**, R567–R570 (1992).
111. J. R. Abo-Shaeer, C. Raman, J. M. Vogels, and W. Ketterle, "Observation of vortex lattices in Bose–Einstein condensates," Science **292**, 476–479 (2001).
112. G. A. Swartzlander and C. Law, "Optical vortex solitons observed in Kerr nonlinear media," Phys. Rev. Lett. **69**, 2503–2506 (1992).
113. W. Firth and D. Skryabin, "Optical solitons carrying orbital angular momentum," Phys. Rev. Lett. **79**, 2450–2453 (1997).
114. D. Skryabin and W. Firth, "Dynamics of self-trapped beams with phase dislocation in saturable Kerr and quadratic nonlinear media," Phys. Rev. E **58**, 3916–3930 (1998).
115. A. Desyatnikov, Y. Kivshar, and L. Torner, "Optical vortices and vortex solitons," Prog. Opt. **47**, 291–391 (2005).
116. K. Dholakia, N. Simpson, M. Padgett, and L. Allen, "Second-harmonic generation and the orbital angular momentum of light," Phys. Rev. A **54**, R3742–R3745 (1996).
117. J. Courtial, K. Dholakia, L. Allen, and M. Padgett, "Second-harmonic generation and the conservation of orbital angular momentum with high-order Laguerre–Gaussian modes," Phys. Rev. A **56**, 4193–4196 (1997).
118. A. Beranskis, A. Matijoius, A. Piskarskas, V. Smilgeviius, and A. Stabinis, "Conversion of topological charge of optical vortices in a parametric frequency converter," Opt. Commun. **140**, 273–276 (1997).
119. R. Ghosh and L. Mandel, "Observation of nonclassical effects in the interference of two photons," Phys. Rev. Lett. **59**, 1903–1905 (1987).
120. D. P. Caetano, M. P. Almeida, P. H. S. Ribeiro, J. A. O. Huguenin, B. C. dos Santos, and A. Z. Khoury, "Conservation of orbital angular momentum in stimulated downconversion," Phys. Rev. A **66**, 041801(R) (2002).
121. M. Marinelli, J. A. O. Huguenin, P. Nussenzveig, and A. Z. Khoury, "Orbital angular momentum exchange in an optical parametric oscillator," Phys. Rev. A **70**, 013812 (2004).
122. G.-L. Oppo, A. J. Scroggie, and W. J. Firth, "Characterization, dynamics and stabilization of diffractive domain walls and dark ring cavity solitons in parametric oscillators," Phys. Rev. E **63**, 066209 (2001).
123. A. Einstein, B. Podolsky, and N. Rosen, "Can quantum-mechanical description of physical reality be considered complete?" Phys. Rev. **47**, 777–780 (1935).
124. J. Howell, R. Bennink, S. Bentley, and R. Boyd, "Realization of the Einstein–Podolsky–Rosen paradox using momentum- and position-entangled photons from spontaneous parametric down conversion," Phys. Rev. Lett. **92**, 210403 (2004).
125. P. G. Kwiat, A. Steinberg, and R. Chiao, "High-visibility interference in a Bell-inequality experiment for energy and time," Phys. Rev. A **47**, R2472–R2475 (1993).

126. A. Mair, A. Vaziri, G. Weihs, and A. Zeilinger, "Entanglement of the orbital angular momentum states of photons," Nature **412**, 313–316 (2001).
127. S. Oemrawsingh, X. Ma, D. Voigt, A. Aiello, E. Eliel, G. 't Hooft, and J. P. Woerdman, "Experimental demonstration of fractional orbital angular momentum entanglement of two photons," Phys. Rev. Lett. **95**, 240501 (2005).
128. J. Leach, B. Jack, J. Romero, A. K. Jha, A. M. Yao, S. Franke-Arnold, D. G. Ireland, R. W. Boyd, S. M. Barnett, and M. J. Padgett, "Quantum correlations in optical angle-orbital angular momentum variables," Science **329**, 662–665 (2010).
129. J. S. Bell, "On the Einstein Podolsky Rosen paradox," Physics **1**, 195–200 (1964).
130. A. Aspect, J. Dalibard, and G. Roger, "Experimental test of Bell's inequalities using time-varying analyzers," Phys. Rev. Lett. **49**, 1804–1807 (1982).
131. J. Leach, B. Jack, J. Romero, M. Ritsch-Marte, R. Boyd, A. Jha, S. M. Barnett, S. Franke-Arnold, and M. J. Padgett, "Violation of a Bell inequality in two-dimensional orbital angular momentum state-spaces," Opt. Express **17**, 8287–8293 (2009).
132. A. Vaziri, G. Weihs, and A. Zeilinger, "Experimental two-photon, three-dimensional entanglement for quantum communication," Phys. Rev. Lett. **89**, 240401 (2002).
133. G. Molina-Terriza, A. Vaziri, J. Řeháček, Z. Hradil, and A. Zeilinger, "Triggered qutrits for quantum communication protocols," Phys. Rev. Lett. **92**, 167903 (2004).
134. J. T. Barreiro, N. K. Langford, N. A. Peters, and P. G. Kwiat, "Generation of hyperentangled photon pairs," Phys. Rev. Lett. **95**, 260501 (2005).
135. E. Nagali, F. Sciarrino, F. D. Martini, L. Marrucci, B. Piccirillo, E. Karimi, and E. Santamato, "Quantum information transfer from spin to orbital angular momentum of photons," Phys. Rev. Lett. **103**, 013601 (2009).
136. E. Karimi, J. Leach, S. Slussarenko, B. Piccirillo, L. Marrucci, L. Chen, W. She, S. Franke-Arnold, M. J. Padgett, and E. Santamato, "Spin–orbit hybrid entanglement of photons and quantum contextuality," Phys. Rev. A **82**, 022115 (2010).
137. L. Deng, H. Wang, and K. Wang, "Quantum CNOT gates with orbital angular momentum and polarization of single-photon quantum logic," J. Opt. Soc. Am. B **24**, 2517–2520 (2007).
138. L. Marrucci, C. Manzo, and D. Paparo, "Optical spin-to-orbital angular momentum conversion in inhomogeneous anisotropic media," Phys. Rev. Lett. **96**, 163905 (2006).
139. G. Biener, A. Niv, V. Kleiner, and E. Hasman, "Formation of helical beams by use of Pancharatnam-Berry phase optical elements," Opt. Lett. **27**, 1875–1877 (2002).
140. G. Calvo and A. Picón, "Spin-induced angular momentum switching," Opt. Lett. **32**, 838–840 (2007).
141. E. Nagali, L. Sansoni, F. Sciarrino, F. D. Martini, L. Marrucci, B. Piccirillo, E. Karimi, and E. Santamato, "Optimal quantum cloning of orbital angular momentum photon qubits through Hong-Ou-Mandel coalescence," Nat. Photonics **3**, 720–723 (2009).
142. E. Brasselet, N. Murazawa, and H. Misawa, "Optical vortices from liquid crystal droplets," Phys. Rev. Lett. **103**, 103903 (2009).

143. S. Khonina, V. Kotlyar, and V. Soifer, "Diffraction optical elements matched to the Gauss–Laguerre modes," Opt. Spectrosc. **85**, 636–644 (1998).
144. S. Khonina, V. Kotlyar, R. Skidanov, V. Soifer, P. Laakkonen, and J. Turunen, "Gauss–Laguerre modes with different indices in prescribed diffraction orders of a diffractive phase element," Opt. Commun. **175**, 301–308 (2000).
145. G. Gibson, J. Courtial, M. Padgett, M. Vasnetsov, V. Pas'ko, S. Barnett, and S. Franke-Arnold, "Free-space information transfer using light beams carrying orbital angular momentum," Opt. Express **12**, 5448–5456 (2004).
146. I. V. Basistiy, V. Bazhenov, M. S. Soskin, and M. V. Vasnetsov, "Optics of light beams with screw dislocations," Opt. Commun. **103**, 422–428 (1993).
147. M. Harris, C. Hill, P. Tapster, and J. M. Vaughan, "Laser modes with helical wave-fronts," Phys. Rev. A **49**, 3119–3122 (1994).
148. M. Soskin, V. Gorshkov, M. Vasnetsov, J. Malos, and N. R. Heckenberg, "Topological charge and angular momentum of light beams carrying optical vortices," Phys. Rev. A **56**, 4064–4075 (1997).
149. I. V. Basistiy, V. Slyusar, M. S. Soskin, M. V. Vasnetsov, and A. Bekshaev, "Manifestation of the rotational Doppler effect by use of an off-axis optical vortex beam," Opt. Lett. **28**, 1185–1187 (2003).
150. J. Leach, M. J. Padgett, S. M. Barnett, S. Franke-Arnold, and J. Courtial, "Measuring the orbital angular momentum of a single photon," Phys. Rev. Lett. **88**, 257901 (2002).
151. J. Leach, J. Courtial, K. Skeldon, S. M. Barnett, S. Franke-Arnold, and M. J. Padgett, "Interferometric methods to measure orbital and spin, or the total angular momentum of a single photon," Phys. Rev. Lett. **92**, 013601 (2004).
152. J. Arlt, "Handedness and azimuthal energy flow of optical vortex beams," J. Mod. Opt. **50**, 1573–1580 (2003).
153. D. Ghai, P. Senthilkumaran, and R. Sirohi, "Single-slit diffraction of an optical beam with phase singularity," Opt. Lasers Eng. **47**, 123–126 (2009).
154. H. Sztul and R. Alfano, "Double-slit interference with Laguerre–Gaussian beams," Opt. Lett. **31**, 999–1001 (2006).
155. G.C.G. Berkhout and M. W. Beijersbergen, "Method for probing the orbital angular momentum of optical vortices in electromagnetic waves from astronomical objects," Phys. Rev. Lett. **101**, 100801 (2008).
156. J. M. Hickmann, E. J. S. Fonseca, W.C. Soares, and S. Chavez-Cerda, "Unveiling a truncated optical lattice associated with a triangular aperture using light's orbital angular momentum," Phys. Rev. Lett. **105**, 053904 (2010).
157. E. Yao, S. Franke-Arnold, J. Courtial, S. Barnett, and M. Padgett, "Fourier relationship between angular position and optical orbital angular momentum," Opt. Express **14**, 9071–9076 (2006).
158. G. Forbes and M. Alonso, "Measures of spread for periodic distributions and the associated uncertainty relations," Am. J. Phys. **69**, 340–347 (2001).
159. S. Franke-Arnold, S. M. Barnett, E. Yao, J. Leach, J. Courtial, and M. Padgett, "Uncertainty principle for angular position and angular momentum," New J. Phys. **6**, 103 (2004).
160. O. Bryngdahl, "Geometrical transformations in optics," J. Opt. Soc. Am. **64**, 1092–1099 (1974).

161. W. Hossack, A. Darling, and A. Dahdouh, "Coordinate transformations with multiple computer-generated optical-elements," J. Mod. Opt. **34**, 1235–1250 (1987).
162. G. C. G. Berkhout, M. P. J. Lavery, J. Courtial, M. W. Beijersbergen, and M. J. Padgett, "Efficient sorting of orbital angular momentum states of light," Phys. Rev. Lett. **105**, 153601 (2010).
163. L. Torner, J. Torres, and S. Carrasco, "Digital spiral imaging," Opt. Express **13**, 873–881 (2005).
164. S. Furhapter, A. Jesacher, S. Bernet, and M. Ritsch-Marte, "Spiral phase contrast imaging in microscopy," Opt. Express **13**, 689–694 (2005).
165. S. Furhapter, A. Jesacher, S. Bernet, and M. Ritsch-Marte, "Spiral interferometry," Opt. Lett. **30**, 1953–1955 (2005).
166. S. Bernet, A. Jesacher, S. Fürhapter, C. Maurer, and M. Ritsch-Marte, "Quantitative imaging of complex samples by spiral phase contrast microscopy," Opt. Express **14**, 3792–3805 (2006).
167. B. Jack, J. Leach, J. Romero, S. Franke-Arnold, M. Ritsch-Marte, S. M. Barnett, and M. J. Padgett, "Holographic ghost imaging and the violation of a Bell inequality," Phys. Rev. Lett. **103**, 083602 (2009).
168. J. H. Lee, G. Foo, E. G. Johnson, and G. A. Swartzlander Jr., "Experimental verification of an optical vortex coronagraph," Phys. Rev. Lett. **97**, 053901 (2006).
169. G. Swartzlander, E. Ford, R. Abdul-Malik, L. Close, M. Peters, D. Palacios, and D. Wilson, "Astronomical demonstration of an optical vortex coronagraph," Opt. Express **16**, 10200–10207 (2008).
170. M. Harwit, "Photon orbital angular momentum in astrophysics," Astrophys. J. **597**, 1266–1270 (2003).

Alison M. Yao graduated from Heriot-Watt University, Edinburgh, and did a Ph.D. at the University of Strathclyde, Glasgow, modeling nonlinear optical systems. She has worked in the Optics Group at the University of Glasgow and is currently a postdoctoral researcher in the Computational and Nonlinear Optics Group at Strathclyde, where her research focuses on quantum entanglement between spatial modes carrying orbital angular momentum.

Miles J. Padgett is Professor of Optics at the University of Glasgow. He heads a 15-person team covering a wide spectrum of projects from blue-sky research to applied commercial development, funded by a combination of government, charity and industry. In 2001 Padgett was elected to Fellowship of the Royal Society of Edinburgh. In 2009 he was awarded the Institute of Physics Young Medal and Prize.